NASA CR-159542

MEASUREMENTS OF ADMITTANCES AND CHARACTERISTIC COMBUSTION TIMES OF REACTIVE GASEOUS PROPELLANT COAXIAL INJECTORS

by

B. A. Janardan

B. R. Daniel

B. T. Zinn

GEORGIA INSTITUTE OF TECHNOLOGY
ATLANTA, GEORGIA 30332

prepared for

NATIONAL AERONAUTICS AND SPACE ADMINISTRATION

NASA Lewis Research Center
Grant NSG-3052
Richard J. Priem, Project Manager

Requests for copies of this report should be referred to:

National Aeronautics and Space Administration
Scientific and Technical Information Facility
P.O. Box 33
College Park, Md. 20740

1 Report No	2. Government Accession No.	3. Recipient's Catalog No
NASA CR-159542		

4 Title and Subtitle	5 Report Date
Measurements of Admittances and Characteristic Combustion Times of Reactive Gaseous Propellant-Coaxial Injectors	March 1979
	6. Performing Organization Code

7. Author(s)	8 Performing Organization Report No
B. A. Janardan, B. R. Daniel and B. T. Zinn	
	10 Work Unit No

9 Performing Organization Name and Address	11. Contract or Grant No
Georgia Institute of Technology School of Aerospace Engineering Atlanta, Ga. 30332	NSG-3052
	13. Type of Report and Period Covered
12 Sponsoring Agency Name and Address	Contractor Report
National Aeronautics and Space Administration Washington D.C. 20546	14. Sponsoring Agency Code

15 Supplementary Notes

Technical Monitor, Richard J. Priem, NASA Lewis Research Center
21000 Brookpark Road, Cleveland, Ohio 44135

16. Abstract

This report describes the results of an experimental investigation that has been concerned with the quantitative determination of the capabilities of combustion processes associated with coaxial injectors to amplify and sustain combustor oscillations. The driving provided by the combustion process was determined by employing the modified standing-wave method utilizing coaxial injectors and air-acetylene mixtures. Analyses of the measured data indicate that the investigated injectors indeed are capable of initiating and amplifying combustion instabilities under favorable conditions of injector-combustion coupling and over certain frequency ranges. These frequency ranges and the frequency at which an injector's driving capacity is maximum are observed to depend upon the equivalence ratio, the pressure drop across the injector orifices and the number of injector elements. In addition to the injector admittances, the characteristic combustion times of coaxial injectors were determined from steady state temperature measurements. Analyses of these data show that the characteristic combustion times also depend upon the frequency, the pressure drop across the injector orifices and the number of injector elements. Also, a good agreement between the measured admittances and the predictions of the Feiler and Heidmann model was obtained when the independently measured characteristic combustion times were substituted into the theoretical analysis.

17. Key Words (Suggested by Author(s))	18 Distribution Statement
Acoustic Instability Admittance Combustion Instability Gaseous Rocket Injector Response Factor	Unclassified-Unlimited

19 Security Classif. (of this report)	20 Security Classif (of this page)	21. No. of Pages	22 Price*
Unclassified	Uncalssified	69	

* For sale by the National Technical Information Service, Springfield, Virginia 22161

NASA CR-159542

MEASUREMENTS OF ADMITTANCES AND CHARACTERISTIC COMBUSTION TIMES OF REACTIVE GASEOUS PROPELLANT COAXIAL INJECTORS

B. A. Janardan

B. R. Daniel

B. T. Zinn

GEORGIA INSTITUTE OF TECHNOLOGY
ATLANTA, GEORGIA 30332

prepared for

NATIONAL AERONAUTICS AND SPACE ADMINISTRATION

NASA Lewis Research Center
Grant NSG-3052
Richard J. Priem, Project Manager

ABSTRACT

This report describes the results of an experimental investigation that has been concerned with the quantitative determination of the capabilities of combustion processes associated with coaxial injectors to amplify and sustain combustor oscillations. The driving provided by the combustion process was determined by employing the modified standing-wave method utilizing coaxial injectors and air-acetylene mixtures. Analyses of the measured data indicate that the investigated injectors indeed are capable of initiating and amplifying combustion instabilities under favorable conditions of injector-combustion coupling and over certain frequency ranges. These frequency ranges and the frequency at which an injector's driving capacity is maximum are observed to depend upon the equivalence ratio, the pressure drop across the injector orifices and the number of injector elements. In addition to the injector admittances, the characteristic combustion times of coaxial injectors were determined from steady state temperature measurements. Analyses of these data show that the characteristic combustion times also depend upon the frequency, the pressure drop across the injector orifices and the number of injector elements. Also, a good agreement between the measured admittances and the predictions of the Feiler and Heidmann model was obtained when the independently measured characteristic combustion times were substituted into the theoretical analysis.

TABLE OF CONTENTS

	Page
INTRODUCTION	1
NOMENCLATURE	4
INJECTOR ADMITTANCE	6
EXPERIMENTAL APPARATUS	10
TEST INJECTORS	13
RESULTS	16
Structure of Standing Wave	16
Nonreactive Coaxial Injector Admittance Data	19
Reactive Coaxial Injector Admittances with Methane-Air as Propellants	21
Reactive Admittances of Coaxial Injectors with Acetylene-Air as Propellants	22
Steady State Temperature Distributions	25
Determination of Characteristic Combustion Time from Temperature Data	26
Comparison of Measured and Predicted Reactive Admittances	29
Effect of Number of Elements on Injector Admittance	30
Empirical Correlations of Self-Driving Periods	31
Porous Plate Injector Admittances	32
CONCLUSIONS	33
ACKNOWLEDGEMENTS	35
REFERENCES	35
TABLES	39
ILLUSTRATIONS	42

LIST OF ILLUSTRATIONS

Figure	Title	Page
1	Effect of Characteristic Combustion Time Upon the Feiler and Heidmann Predicted Admittances.	42
2	Sectional View of the Test Apparatus	43
3	Instrumentation System	44
4	Pictorial View of the Experimental Apparatus	45
5	Experiment Control Area	46
6	Coaxial Injector: Configuration # 1 (26 Injector Elements).	47
7	Coaxial Injector: Configuration # 2 (13 Injector Elements).	47
8	Pictorial View of Coaxial Injector Configuration # 1	48
9	Porous Plate Injector: Configuration # 3	49
10	Axial Dependence of Pressure Amplitude and Phase: Coaxial Injector Configuration # 1, Flow Series 2, Equivalence Ratio = 1.31; Driver Frequency = 954 Hz.	50
11	Axial Dependence of Pressure Amplitude and Phase: Coaxial Injector Configuration # 1, Flow Series 2, Equivalence Ratio = 1.31; Driver Frequency = 805	51
12	Axial Dependence of Pressure Amplitude and Phase: Coaxial Injector Configuration # 1, Flow Series 2, Equivalence Ratio = 1.31; Frequency = 750 Hz.	52
13	Dependence of Non-Reactive Admittances of Coaxial Injector Configuration # 2 upon Propellant Flow Rates	53

14	Effect of Number of Elements in Coaxial Injectors upon Non-Reactive Admittances: Flow Series 2	54
15	Comparison of Measured Non-Reactive and Reactive Admittances of Coaxial Injector Configuration # 1: Fuel-Methane, Flow Series 4	55
16	Comparison of Measured Reactive with Non-Reactive Admittances of Coaxial Injector Configuration # 2: Flow Series 2, Equivalence Ratio = 0.57	56
17	Comparison of Reactive with Non-Reactive Admittances of Coaxial Injector Configuration # 1: Flow Series 2, Equivalence Ratio = 0.57	57
18	Frequency Dependence of Reactive Admittance of Coaxial Injector Configuration # 1; Flow Series 2, Equivalence Ratio = 1.02	58
19	Frequency Dependence of Reactive Admittance of Coaxial Injector Configuration # 1: Flow Series 2, Equivalence Ratio = 1.31	59
20	Dependence of Measured Admittances of Coaxial Injector Configuration # 1 upon Propellant Flow Rates: Equivalence Ratio = 0.57	60
21	Comparison Between Measured and Predicted Reactive Admittances of Coaxial Injector Configuration # 2: Flow Series 2, Equivalence Ratio = 0.57	61
22	Measured Steady State Coaxial Temperature Distributions in the Vicinity of Injector Configuration # 2 at Different Test Frequencies Flow Series 1: (1) Equivalence Ratio = 0.57, (b) Equivalence Ratio = 1.02	62

23	Frequency Dependence of the Characteristic Combustion Time of Coaxial Injector Configuration # 2 Obtained From Steady State Temperature Measurements	63
24	Frequency Dependence of the Characteristic Combustion Time of Coaxial Injector Configuration # 1 Obtained From Steady State Temperature Measurements	64
25	Comparison Between Measured Reactive Admittances of Coaxial Injector Configuration # 2 with Predicted Reactive Admittances Obtained with τ_b^* that is Calculated from Temperature Data: Flow Series 2	65
26	Effect of Number of Elements in Coaxial Injectors Upon Measured Reactive Admittances: Flow Series 2, Equivalence Ratio + 0.57	66
27	Dependence of Self-Excitation Half-Period of Coaxial Injector Configuration # 1 Upon Equivalence Ratio: Oxidizer Flow of Series 2	67
28	Dependence of Self-Excitation Half-Period of Coaxial Injector Configuration # 2 Upon Equivalence Ratio: Oxidizer Flow of Series 2 and 3	68
29	Measured Admittance Data of Injector Configuration # 3: Flow Series 2	69

LIST OF TABLES

Table	Title	Page
I	Operating Flow Rates	39
II	Test Matrix	40
III	Self-Driving Test Results	41

INTRODUCTION

Rocket motors, gas turbine combustors and industrial burners are subject to combustion instabilities that involve oscillations of the gases within their combustion chambers. Such instabilities can be classified broadly under three categories[1]; namely, system, combustion-chamber and intrinsic instabilities. System instabilities result when there is an interaction between the processes occurring in the combustion chamber and those occurring in another component of the system. Common examples of such instabilities are those observed in liquid and gaseous rocket motors and gaseous fuel fired burners wherein there is an interaction between the combustion process and the wave motions within the feed system and the combustion chamber. On the other hand, combustion-chamber and intrinsic instabilities are those that are specific to the combustion chamber and reactants, respectively.

Considerable effort has been devoted in recent years to the analyses of combustion instability problems. One of the main objectives of these investigations has been the development of quantitative data that could be used to determine whether a given combustor disturbance would attenuate or amplify, thus resulting in a stable or unstable combustor operation. Of primary importance in such investigations was the determination of the attenuation or damping provided by system components such as nozzles and mechanical damping devices and the amplification or driving provided

by the injector and its associated combustion process. Customarily, the effect of each of the above-mentioned processes on chamber stability can be determined from its response factor that describes the process response to a given disturbance. The real and imaginary parts of this response factor describe the relationships that exist between the amplitudes and phases of the heat or mass flow rate perturbation that are associated with the process under consideration, and the local pressure perturbation. The contribution of a given process to the overall stability of the system is determined by multiplying the real part of its response factor by a weighting factor that takes into consideration the relative contribution of this process to the system stability.[2] This multipliation is performed for all relevant system processes and the sum of the resulting products are determined. In this summation, driving and damping processes provide respectively positive and negative contributions. When this sum is positive, indicating a net in-phase heat or mass addition, the combustor is unstable. Conversely, the combustor is stable when this sum is negative implying a net out-of-phase heat or mass addition relative to the pressure oscillation. It is to be noted here that this response factor approach of stability analysis is consistent with the Rayleigh criterion which states that an oscillation will grow or decay when heat or mass is added in-phase or out-of-phase with the pressure perturbation, respectively.

The attenuation provided by nozzles and mechanical damping devices have been considered in a number of earlier investigations.[3-7] In contrast, little work has been done to date to determine the influence of the injector design upon the combustor stability. In an effort to determine whether coupling between propellant flow rate oscillations and the chamber pressure oscillations could provide a mechanism for driving combustion instabilities, Feiler and Heidmann[2] and Priem and Yang[8] have analytically studied the unsteady flow behavior of gaseous injector elements. The results obtained in these analytical studies and related experimental studies[9-12] suggest that injector-combustor coupling and the resulting fluctuations in the rate of heat release could be the cause of instabilities in combustion chambers. A related problem has been investigated by Sipowicz et al.[13] who employed a modified T-burner with a permeable injector and a premixed gaseous propellant. The results of this study have suggested the need to consider gas phase kinetics to explain the amplifying characteristics of combustion systems. In addition, experiments performed by Toong et al.[14] and Jarosinski et al.[15] have shown that the onset of flame oscillations due to flow instabilities, like vortex shedding and transition between laminar and turbulent flow, can result also in amplification of acoustic oscillations in combustors. Although these and other experimental studies do provide some insight into the mechanism of combustion driven oscillations, they do not provide data that can be used to check the predictions of available theoretical models, or be used as inputs during stability

analyses.

This report describes the results of an investigation that has been undertaken in an effort to provide such information. In this case the modified standing-wave technique has been utilized to measure gaseous coaxial injector response factors under a variety of reactive conditions*. Subsequently, the measured data have been compared with the corresponding analytical predictions of Ref. 2 and the effect of injector design parameters upon combustion stability has been investigated. The experimental approach, the measured data and the comparisons with available theoretical predictions are described in this report.

NOMENCLATURE

A	area
C	Capacitance, defined by Eq. (9)
c	speed of sound
I	Inductance, defined by Eq. (9)
L	length of the injector orifice
M	Mach number
N	injector response factor

---

* The terms reactive and nonreactive, denoted by R and NR, are used to describe injector flow conditions with and without combustion, respectively.

P	pressure
q	equivalence ratio
R	Resistance, defined by Eq. (9)
U	velocity
V	injector dome volume
W	mass flow rate of propellant
Y	admittance
γ	specific heat ratio
δ	equal to $(\bar{P}^*_d - \bar{P}^*_c)/\bar{P}^*_c$
ρ	density
σ	open-area ratio of the injector
τ	characteristic combustion time
ω	angular frequency

Superscripts

$\bar{(\ )}$	steady state quantity
$(\ )^*$	dimensional quantity
$(\ )'$	perturbation quantity

Subscripts

$(\ )_b$	associated with the combustion process
$(\ )_c$	evaluated in the chamber
$(\ )_d$	evaluated in the injector dome
$(\ )_f$	associated with the fuel
$(\ )_{ox}$	associated with the oxidizer
$(\ )_1$	evaluated at injector orifice entrance

$()_2$ evaluated at injector orifice exit

INJECTOR ADMITTANCE

Available experimental investigations of the behavior of injectors[7,16] indicate that the steady state gas flow and heat transfer patterns inside the combustion chamber are dependent upon the design of the injector elements. In addition, the injector design influences the response of the propellants' burn rate to combustors oscillations. This interaction of the injector-combustion process with the combustor oscillation is normally described by either the injector response factor N^* or the admittance Y^* which are defined respectively, as the complex ratio of the burning rate perturbation or the normal velocity perturbation to the local pressure perturbation; that is

$$N^* = \frac{\vec{W}^{*\prime} \cdot \vec{n}}{P^{*\prime}} \tag{1}$$

and

$$Y^* = \frac{\vec{U}^{*\prime} \cdot \vec{n}}{P^{*\prime}} \tag{2}$$

The nondimensional form of the injector response factor and the admittance can be written in the following form

$$N = \frac{\vec{W}^{*\prime} \cdot \vec{n}/\bar{W}^*}{P^{*\prime}/\bar{P}^*} \tag{3}$$

$$Y = \frac{\vec{U}^{*\prime} \cdot \vec{n}}{\bar{\rho}^{*} \cdot \bar{c}^{*} \; P^{*\prime}} \tag{4}$$

where the reference admittance $1/\bar{\rho}^{*}\bar{c}^{*}$ is the characteristic admittance of the gas medium at the injector face. From the above definitions, the following expression[17,18] relating the nondimensional response factor N to the nondimensional admittance Y can be obtained:

$$N = \frac{1}{\gamma \bar{M}} \left\{ Y + \vec{M} \cdot \vec{n} \right\} \tag{5}$$

In an effort to develop a theoretical model for predicting the response factor of a gaseous injector Feiler and Heidmann[2] analyzed the unsteady flow behavior in a gaseous hydrogen coaxial injector element. The response of the injector flow rate to a small amplitude pressure oscillation in the chamber was determined by manipulating the linearized conservation equations for each of the injector components. Assuming that each of the injector components behaves as a lumped element and that the combustion was concentrated in front of the injector exit plane, the following expression for the injector response factor N was obtained[2]:

$$N = \frac{W_b'}{P_c'} = \left\{ \frac{W_b'_{max}}{P_c'_{max}} \right\} e^{i\theta} \tag{6}$$

where

$$\frac{W'_{b_{max}}}{P'_{c_{max}}} = \frac{-1}{R_2\left\{\left[\frac{R_1}{C^*\omega^*} - I^*\omega^*\right]^2 + \left[2\left(\frac{R_1\Delta P_1^*}{\bar{P}_d^*} + \frac{\Delta P_2^*}{\bar{P}_2^*}\right)\right]^2\right\}^{\frac{1}{2}}} \tag{7}$$

$$\theta = \frac{\pi}{2} - \omega^*\tau_b^* - \arctan\frac{2\left\{\frac{R_1\Delta P_1^*}{\bar{P}_d^*} + \frac{\Delta P_2^*}{\bar{P}_2^*}\right\}}{\left\{\frac{R_1}{C^*\omega^*} - I^*\omega^*\right\}} \tag{8}$$

and

$$C^*\omega^* = \left[\bar{\rho}_d^* V^*/\gamma\bar{W}^*\right]\omega^* \quad ; \quad I^*\omega^* = \left\{\bar{W}^*\left[L^*/A_1^*\right]/g\bar{P}_2^*\right\}\omega^* \tag{9a}$$

$$\frac{\Delta P_1^*}{\bar{P}_d^*} = \left\{\bar{P}_d^* - \bar{P}_1^*\right\}/\bar{P}_d^* ; \quad \frac{\Delta P_2^*}{\bar{P}_2^*} = \left\{\bar{P}_2^* - \bar{P}_c^*\right\}/\bar{P}_2^* \tag{9b}$$

$$R_1 = \frac{\bar{P}_d^*}{\bar{P}_1^* - \left\{\Delta P_1^*/\gamma\right\}} \quad ; \quad R_2 = \frac{\bar{P}_2^*}{\bar{P}_c^* - \left\{\Delta P_2^*/\gamma\right\}} \tag{9c}$$

The quantity τ_b^* appearing in Eq. (8) represents the residence time of a propellant mass element in the combustor prior to its combustion. The above expressions describe the dependence of the injector response factor upon the injector geometry, flow conditions in the chamber and the injector, and the characteristic combustion time. Subsequently, this model has been modified by Priem and Yang[8] to

account for the compressibility of the gaseous streams flowing through the injector elements.

The results of the Feiler and Heidmann analysis indicate that the magnitude of τ_b^* is a controlling factor in the stability of a given combustor. When there is no combustion present in the system, τ_b^* is zero and the results of Ref. 2 then indicate that the basic injector-chamber system is inherently stable. This result has been verified in an earlier cold flow study[18] conducted by the authors of this report. However, for situations when combustion is present in the system the Feiler and Heidmann model shows that various injector designs can amplify and sustain chamber oscillations for certain ranges of the parameter τ_b^*. This is illustrated in this section by presenting the Feiler and Heidmann predicted admittances for one of the coaxial test injector configurations of this study. This test injector has 26 injector elements with a total oxidizer open-area ratio of 6% and a total fuel open-area ratio of 0.5%. The predicted frequency dependence of the surface admittance of the test injector configuration for a given flow rates of propellants is presented in Fig. 1 for four different values of τ_b^* ; namely, 0.0, 0.6, 0.7 and 0.8 msec. An examination of this figure indicates that, for the nonreactive case of $\tau_b^* = 0.0$, the predicted real part of the complex admittance is a positive number over the entire test frequency range. However, for the reactive cases with τ_b^* equal to 0.6, 0.7 and 0.8 msec, the real parts of the complex admittances are predicted to be negative

numbers over certain ranges of the frequency. It can be shown that a positive real part of the complex injector admittance implies wave damping at the injector surface while a negative real part implies wave amplification or driving at the injector end. Thus, the Feiler and Heidmann model predicts that under reactive conditions injectors can act as driving devices over certain frequency ranges. It is one of the objectives of this investigation to provide experimental data that could be used to check this prediction.

In spite of its indicated importance, the combustion time τ_b^* is generally not known and, to date, little effort has been made to measure it.[19,20] To provide the needed data, part of the effort conducted under this study has been devoted to the determination of the combustion time τ_b^*. The experimental approach and the measured results are presented in following sections of this report.

EXPERIMENTAL APPARATUS

The injector surface admittance data, from which the required injector response factors can be evaluated, are determined in this study by using the modified impedance-tube or standing-wave technique. In this method, a sound source capable of generating simple harmonic waves of desired frequencies is placed at one end of a simulated combustion chamber and the injector system under investigation is placed at the other end. During an experiment, the acoustic driver generates a plane wave which propagates toward the test injector elements. The interaction of this wave with the injector

elements and the combustion process results in either amplification or attenuation of the incident wave. The reflected wave interacts with the incident wave to form a standing wave pattern in the impedance tube.

The structure of the impedance tube standing wave depends upon the admittance at the injector end, the frequency of the wave, the mean flow Mach number and steady flow inhomogeneities due to the presence of an axial temperature gradient caused by heat transfer to the tube walls. To determine the unknown injector admittance, which is one of the objectives of this study, the admittance values that provide the best fit between experimental data consisting of acoustic pressure measurements and analytical solutions that describe the wave structure in the tube are computed. The characteristics of the acoustic wave structure under the above described environments have been investigated analytically in Refs. 21-23. In addition, Ref. 23 presents a data reduction scheme which allows one to use measured acoustic pressure data in the determination of the injector admittances. This scheme has been used in the present study and it involves the determination of both the steady flow gradients and the injector admittance that provide the best fit between the measured data and analytically predicted standing wave structure.

The apparatus, schematically shown in Fig. 2, consists of a 4 inch diameter stainless steel simulated combustor with a sound

source at one end and the test injector system at the other end. Continuous and steady flow of the required fuel and oxidizer are obtained from pressurized storage cylinders. The acoustic pressure wave structure and the steady temperature behavior are determined by installing dynamic pressure transducers and thermocouples at desired locations along the walls of the combustor. During a test, the required flows of oxidizer and fuel are first established in the combustor and combustion is then initiated by means of a propane-air torch situated a short distance downstream of the injector face. A standing wave of a known frequency and having a maximum sound pressure level between 166 and 160 dB is next established by employing the acoustic drivers. Upon stabilization of flow conditions in the combustor, the standing wave structure and steady temperature behavior along the combustor is measured by axially moving the combustor tube, in short steps of known magnitude, relative to the injector and acoustic drivers that remain fixed in their positions. The axial movement of the combustor tube is achieved by a tube translation system consisting of a stepping motor and a lead screw drive. Utilizing five pressure transducers spaced 8 inches apart and two thermocouples, the needed acoustic pressure wave structure in the tube and the steady temperature distribution in the vicinity of the injector are determined by translating the combustor walls a distance of eight inches. The analog data, taken at each step, are suitably amplified, analyzed and digitized in an analog to digital

convertor and then stored on a cartridge disc of a minicomputer. The details of the instrumentation system employed in this study are described in Figure 3. Also, pictorial views of the apparatus and the instrumentation used during this program are, respectively shown in Figs. 4 and 5.

The digitized and stored data of each run are printed and plotted later and fromwhich the desired admittance value is computed by the use of a nonlinear regression analysis that provides a best fit between a discrete number of acoustic pressure measurements along the tube and the corresponding analytically predicted wave structure.[23] This procedure is repeated at different driver frequencies to determine the frequency dependence of the test injector admittance.

TEST INJECTORS

The test injector configurations investigated during this study are shown in Figs. 6-9. Configurations # 1 and # 2, that are respectively described in Figs. 6 and 7, are designed to simulate the flow behavior through gaseous fuel coaxial injector elements. Both of these configurations are geometrically identical with an oxidizer open-area ratio of 6 percent and a fuel open arearatio of 0.5 percent. These injectors have been designed so that the oxidizer elements response factors, as predicted by Ref. 2, are much larger than the fuel elements response factors over the test frequency range. Also,

the operating oxidizer flow rates are much larger than the operating fuel flow rates. A direct consequence of this design is that the measured total injector admittance is in effect the admittance of the oxidizer elements only, as the fuel elements contribute insignificantly to the measured admittance. However, in order to determine the dependence of the injector admittance upon the size of the individual injector elements, configurations # 1 and # 2 are respectively designed to have 26 and 13 individual injector elements. A pictorial view of the 26 elements injector is presented in Fig. 8.

Injector configuration # 3, shown in Fig. 9, has been designed with the objective to determine the admittance of an injector configuration wherein the oxidizer dome is decoupled from the oscillations in the combustor. This is achieved by having the oxidizer pass from the plenum chamber of the injector into the combustor through a porous plate. Since a plate with a low porocity has been employed, a large pressure drop across the injector plate is required to maintain the needed oxidizer flow rate. This large pressure drop across the injector plate results in decoupling the oxidizer dome from chamber oscillations. A similar injector has been designed and tested in Ref. 24 with a view to improve the reliability and simplify the fabrication procedures of injector elements.

During this study, a series of experiments have been conducted under both reactive and nonreactive conditions with compressed air as the oxidizer. While acetylene was employed as the fuel during most

of these tests, some experiments were also conducted with methane as the fuel. In each case, steady state experiments were first conducted with the test injectors so as to determine their operating range in terms of the blow-off velocity and equivalence ratio. With the range of the injector operating flow conditions known, tests were conducted next to measure the response of the injector system at a given equivalence ratio. These experiments included three series of tests with acetylene as the fuel during each of which the oxidizer flow rate W^*_{ox} has been kept fixed and the required test equivalence ratios have been obtained by suitably varying the fuel flow rate W^*_f. This required that the pressure drop ΔP^*_{ox} across the injector oxidizer orifices be maintained constant during each of the series of tests. Conducting these three series of tests with three different oxidizer flow rates and three different ΔP^*_{ox} allowed for the determination of the dependence of the injector admittance and the value of τ^*_b upon ΔP^*_{ox} and equivalence ratio. The mass flow rates utilized in these three series of tests with acetylene and the remaining fourth series with methane as the fuel are summarized in Table I. A test matrix describing the flow conditions under which each of the three injector configurations has been tested is presented in Table II. The combustion chamber pressure was maintained at one atmosphere during all of these tests.

RESULTS

Structure of Standing Wave

Before examining the injector admittance data, some comments regarding the structure of the standing wave in the impedance tube are in order. Theoretical studies show that the characteristics of the impedance tube standing wave are dependent, among many other parameters, upon the nature of the admittance boundary condition at the injector end. When the real part of this complex admittance is a positive number, which implies wave damping at the injector face, the phase distribution along the impedance tube has a positive slope indicating the propagation of acoustic energy towards the injector end. On the other hand, when the real part of the complex admittance is negative in sign, which implies wave amplification at the injector end, the phase-distance curve in the burner tube has a negative slope indicating transmission of acoustic energy away from the injector. Using this information, a knowledge of the slope of the phase-distance curve can be used to determine the sign of the real part of the admittance at the injector end. It can also be shown that the ratio of the maximum to the minimum sound pressure levels of the standing wave in the impedance tube is a measure of the magnitude of the real part of the admittance and vice versa.

Typical plots describing the axial distribution of the pressure amplitudes and phases measured with injector configuration # 1 having propellants flow rates of series 2 are presented in Figs. 10-12.

The data presented in these figures compare the pressure amplitudes and phases measured under nonreactive conditions and at driver frequencies of 954, 805 and 750 Hz with corresponding data obtained under reactive conditions. An examination of the phase data of Fig. 10 indicates that the phase-distance curves measured at the driver frequency of 954 Hz have a positive slope under both reactive and non-reactive conditons. This in turn indicates that the acoustic energy was moving from right to left along the burner tube and hence the injector was acting as a damping device under both reactive and nonreactive conditions. However, an examination of the amplitude curves in Fig. 10 indicates that a decrease in the damping provided by the injector occurred when the operating condition of the system changed from a non-reactive to a reactive state. A similar examination of Fig. 11, obtained with a driver frequency of 805 Hz, indicates that while the phase-distance curve under non-reactive conditions has a positive slope, the phase-distance curve under reactive conditions has a small negative slope. This indicates a change in the direction of the acoustic energy propagation in the impedance-tube as the system changed from a non-reactive to a reactive condition. In other words, this indicates a change from a damping to mild driving response factor at the injector face. Figure 12, describing the data obtained at a driver frequency of 750 Hz, also indicates that the nature of the phase-distance curve changes from a positive to a negative slope as the operating condition of the system

is changed from a nonreactive to a reactive state.However, the phase-distance curve of Fig. 12 has a considerable larger negative slope when compared to the almost square looking phase-distance curve of Fig. 11. This indicates a stronger driving capability at 750 Hz when compared to that at 805 Hz. This trend is also evident from a comparison of the reactive pressure amplitude data of Fig. 12 with the corresponding reactive data of Fig. 11.

To assure the repeatability of the measured data, the axial distributions of the pressure amplitudes and phases have been measured in repeated tests for a number of different oxidizer and fuel flow rates and test frequencies. One set of such data obtained under both reactive and nonreactive conditions are presented in Fig. 12. An examination of this figure indicates that the measured amplitudes and phases indeed are repeatable. In this connection it should be pointed out that the geometry of the injector under investigation and its operating flow rates were selected so as to yield injector admittances that result in a standing wave in the impedance tube with less than 40 dB difference between the maximum and minimum pressure amplitudes over the test frequency range. Since the inherent flow noise in the impedance tube was measured at a 120 dB level, all the experiments were conducted with a standing wave maximum pressure amplitude in the range 160-166 dB so as to minimize the effect of noise on the quality of the data at the pressure minima.

Nonreactive Coaxial Injector Admittance Data

The results presented in this section were obtained by measuring the frequency dependence of the admittances of the test configurations # 1 and # 2 under the nonreactive flow conditions described in Table I and over a frequency range of 200 to 1000 Hz. This frequency range includes the nonreactive resonant frequencies of the two injectors. The measured nonreactive admittance data for injector configuration # 2 are presented in Fig. 13 along with the corresponding predictions of the Feiler and Heidmann[2] model which were obtained utilizing a corrected orifice effective length as suggested in Ref. 18. An examination of this figure indicates a reasonably good agreement between the measured and predicted data. A similar agreement between the measured and predicted nonreactive admittances for injector configuration # 1 was also obtained.

The above presented data indicate that, for the nonreactive case, both the predicted and measured real parts of the admittances are positive over the entire test frequency range. As earlier mentioned, a positive real part of the complex injector admittance implies wave damping at the injector surface while a negative real part indicates wave driving at the injector end. Hence, the presented nonreactive admittance data indicate that the injector acts as a mechanical damping device under all nonreactive conditions. Further examination of the data indicates a significant decrease in the magnitude of the injector surface admittance and hence the amount

of wave damping near the resonant frequency with an increase in the oxidizer mass flow rates through the injectors. An increase in the oxidizer mass flow rates for a given injector results in an increase in the pressure drop across the oxidizer orifices which result in an increase in the injector resistance. This in turn decreases the coupling between the pressure oscillation inside the injector dome and the pressure oscillation in the combustor. However, the increase in the pressure drop is observed to have little effect upon the injector resonant frequency.

A comparison of the frequency dependence of the nonreactive admittances of the two coaxial injectors is presented in Fig. 14 for the series 2 oxidizer flow rates. It should be recalled that both of these configurations are geometrically identical except for the number of injector elements. Configuration # 1 contains 26 injector elements while configuration # 2 has 13 injector elements. Also, the data presented in Fig. 14 are for identical flow rates through the two injectors. An examination of this figure indicates that the resonant frequency of configuration # 2 is less than that of configuration # 1 thereby indicating a longer orifice effective length for configuration # 2 when compared to that of configuration # 1. Also, the maximum value of the real part of the nondimensional admittance of configuration # 2 is larger than the corresponding data of configuration # 1. A similar observation made also by comparing the nonreactive data of the test injectors for series 1 and series 3 flow

rates. This inequality in admittance data appears perplexing, at the outset, because of the fact that the two injectors have the same geometrical dimensions and have been tested at equal oxidizer flow rates. However, it should be noted that the individual oxidizer orifices of configuration # 2 are larger than those of configuration # 1 and hence the coefficients of discharge for the two sets of injectors could be different. In that case, equal oxidizer flow rates through the two injectors would result in different pressure drops across the injector oxidizer orifices and hence different oxidizer element resistances. A pressure measurement across the orifices of the two injectors for the series 2 flow rates confirmed the existence of different pressure drops across the oxidizer elements. For injector configuration # 1, the nondimensional pressure drop δ_{ox} across the oxidizer elements, normalized using the simulated chamber pressure, was measured to be 0.0065 while the coresponding data for configuration # 2 was found to be 0.0044. From the measured flow rates and the pressure drops, the coefficients of discharge were computed to be 0.61 and 0.74 for the configurations # 1 and # 2, respectively. Hence, for a given open area-ratio and flow rates, increasing the orifice size can result in a decrease in the nonreactive resonant frequency and an increase in the coupling between the flow oscillations and chamber pressure oscillations .

Reactive Coaxial Injector Admittances With Methane-Air as Propellants

During the initial period of this investigation, some limited

number of tests were conducted using methane as the fuel. The mass flow rates for this series of tests are described in Table I and the measured reactive and nonreactive admittances are presented in Fig. 15. An examination of this figure indicates that the real parts of the admittances are positive over the test frequency range indicating that the test systems could not amplify or sustain combustion instabilities under reactive conditions. However, further examination of this figure indicates that a considerable decrease in the damping provided by the injector occurred when the operating conditions of the system changed from a nonreactive to a reactive state. Additional tests at other air and methane flow rates indicated the inability of this methane-injector system to drive or sustain combustion oscillations in the impedance tube. Since measurement of the driving admittances was one of the prime objectives of this study and tests with acetylene as the fuel indicated the driving ability of the system under varied flow conditions, it was decided to conduct the required experiments with only acetylene as the fuel. These data are presented and discussed in the remaining sections of this report.

Reactive Admittances of Coaxial Injectors With Acetylene-Air as Propellants

To establish the repeatability of the measured reactive admittance data, the frequency dependence of the admittance of injector configuration # 2 with operating flow rates corresponding to series 2 and an equivalence ratio of 0.57 (i.e., see Table 1) has been

measured on two different occasions. The fairly good repeatability of the measured admittances is demonstrated by the data presented in Fig. 16. For comparison purposes, Fig. 16 also contains the corresponding nonreactive admittances. Comparison of these two sets of data indicates that, while the real parts of the nonreactive admittances are positive over the entire test frequency range, the real parts of the reactive admittances are negative over a certain frequency range only. This implies that the combustion process associated with a given injector can amplify and sustain combustion instabilities over certain frequency ranges only.

Similar data have been obtained at other operating conditions of this study except that the frequency range for which a given coaxial injector is able to drive the combustor oscillations is different for different oxidizer and fuel flow rates. This is demonstrated by the admittance data presented in Figs. 17-20. Figures 17-19 describe the frequency dependence of the admittance of injector configuration # 1 with a constant oxidizer flow rate of series 2 and fuel flow rates adjusted to give equivalence ratio of 0.57, 1.02 and 1.31 respectively. An examination of these three figures indicates that the driving frequency ranges are different for the different equivalence ratios. Furthermore, a decrease in the magnitude of the negative maximum of the real part of the complex admittance is observed with an increase in the equivalence ratio. Similarly, the admittance data of configuration # 1 obtained at the two different oxidizer flow rates of series 1 and 2 are compared with each other in Fig. 20 for an

equivalence ratio of 0.57. An examination of this figure also indicates that the driving frequency ranges and the magnitude of the negative maximum of Y are different for the different oxidizer flow rates. Similar trends have also been observed with the injector configuration # 2 and those data are presented in a later section of this report.

Figure 17, describing the frequency dependence of the surface admittance of configuration # 1 with series 2 oxidizer flow rate and an equivalence ratio of 0.57, also contains for comparison purposes the corresponding Feiler and Heidmann predicted admittances. The predicted data have been obtained for three different assumed values of τ_b^* ; namely, 0.6, 0.7 and 0.8 msec. A comparison of the measured data with the predicted admittances indicates a good agreement between the two sets of data when τ_b^* equals 0.7 msec in the Feiler and Heidmann anaysis. Similarly, comparing the measured admittances with the predicted data for the above mentioned series of tests but with equivalence ratios of 1.02 and 1.31 indicate that the two sets of data agree qualitatively where the values of τ_b^* are taken to be 0.85 and 1.2 msec respectively. However, an examination of Figs. 18 and 19 indicates a certain amount of scatter in the measured data.

A similar observation has also been made with the admittance data of the coaxial injector configuration # 2 . This is illustrated in Fig. 21 wherein the measured real part of the reactive admittance data of Fig. 16 is compared with the corresponding predictions of the

Feiler and Heidmann model obtained for three different assumed values of the characteristic combustion time τ_b^*; namely 0.8, 1.0 and 1.2 msec. An examination of this figure indicates that all of the measured data are scattered around the theoretically predicted curve with τ_b^* equal to 1.0 msec and in a region enveloped by the two remaining curves. This observation suggests that for the given injector operating conditions the Feiler and Heidmann model can only qualitatively predict the reactive admittance behavior, or that the magnitude of τ_b^* is frequency dependent and it varies between 0.8 and 1.2 msec for the indicated frequency range. Similar observations have also been made for the other operating flow conditions investigated in this study except that the range of "matching" values are different for each of these cases. The resolution of this problem is considered in the following sections.

Steady State Temperature Distributions

The experimental apparatus section discussed the use of thermocouples to measure the steady state temperature distribution $\bar{T}^*(x)$ in the vicinity of the injectors during each reactive test run. A typical set of measured temperature data obtained in the vicinity of injector configuration # 2 for a couple of series 1 flow rates are presented in Fig. 22. An examination of this figure and other temperature data measured in the course of this study indicates that for a given equivalence ratio the temperature distributions and the parameter L^*_{tmax}, which measures the axial distance from the

injector face to the point of maximum temperature, are generally frequency dependent. Considering the physics of the investigated combustion processes, it will be shown next that this observation implies that the characteristic combustion time τ_b^* is also frequency dependent.

Determination of Characteristic Combustion Time from Temperature Data

It has been stated earlier in this report that the characteristic combustion time τ_b^* is a measure of the propellants residence time in the combustor prior to complete combustion. A value of τ_b^* has been calculated [7] previously by determining the flight time of a propellant element from the injector face to the point of complete combustion. Hence, if the location of the plane of maximum steady state temperature is also an indication of the plane of complete combustion then a value of τ_b^* can be obtained by calculating the travel time of a propellant element between the injector face and the location L_{tmax}^*. However, in order to proceed with such a calculation one needs to obtain an effective flow velocity that is consistent with the steady state property distributions over the distance L_{tmax}^*. Specifically, one needs to keep in mind that in the short region extending from the injector face to the plane of complete combustion the steady state temperature varies from the inlet room temperature $\bar{T}_i^*$ to the maximum measured temperature $\bar{T}_c^*$.

A relatively simple minded approach has been tried in the

present study to estimate τ_b^* . Accordingly, the characteristic combustion time has been estimated by letting the average temperature $\bar{T}^*$, equals to $(\bar{T}_i^* + \bar{T}_c^*)/2$,represent the characteristic temperature of the region extending from the injector face to the plane of maximum temperature. Using this average temperature and the known chamber pressure an average density of the propellant is first calculated. The effective propellant flow velocity is then computed from the known propellants flow rate, injector orifice sizes and their coefficients of discharge and the above calculated average density. This velocity together with the measured distance L_{tmax}^* is used then to determine τ_b^* . That this procedure is applicable for the present case is shown in the next section.

The frequency dependence of the characteristic combustion time, obtained from the propellant flight time, is shown in Fig. 23 for tests with injector configuration # 2 and for the three flow rates using acetylene as fuel. An examination of this data indicates that the characteristic combustion time for a given equivalence ratio is frequency dependent and it decreases in magnitude with an increase in frequency. This dependency on the frequency is more predominant for the series 1 runs than for the series 2 and 3 tests. Also, the magnitudes of τ_b^* for the series 3 tests are smaller than those of the series 2 runs which in turn are smaller than those obtained during series 1 tests. In this connection it might be useful to recall that series 1, 2 and 3 tests correspond, respectivey, to higher oxidizer

flow rates and correspondingly larger pressure drops across the oxidizer orifices. This, in turn, implies larger port velocities which in addition to decreasing the flight time also result in increased turbulence and thus a decrease in mixing times. This, therefore, indicates that the larger the pressure drop across the injector orifices the smaller the characteristic combustion time τ_b^* for a given fuel-oxidizer system. In addition, data obtained during series 3 tests indicate little effect of equivalence ratio upon the value of τ_b^*. This implies that for tests with larger pressure drops equivalence ratio has little effect upon the value of τ_b^*.

Similar data obtained with injector configuration # 1 having some of the flow rates described in Table I are presented in Fig. 24. An examination of this figure also indicates that the characteristic combustion time, for a given injector, is dependent upon the equivalence ratio and frequency. However, the dependency on frequency is not as predominent as it was in the case of injector configuration # 2. Also, a comparison between the characteristic combustion times of coaxial injector configurations # 1 and # 2 indicates that, for a given flow rate and equivalence ratio, the τ_b^* values of configuration # 1 are smaller than those of configuration # 2. It is useful to recall at this point that configurations # 1 and 2 have, respectively, 26 and 13 injector elements and that for a given oxidizer flow rate the pressure drop across the orifices and hence the port velocities are larger for injector configuration # 1 when

compared to those of configuration # 2. Larger port velocities combined with a greater number of individual smaller elements leads to a decrease in the flight and mixing times and hence the observed smaller τ_b^* values for injector configuration # 1 when compared to those of configuration # 2.

Comparison of Measured and Predicted Reactive Admittances

To check their applicability, the frequency dependent characteristic combustion times determined from the steady state temperature data were substituted into the Feiler and Heidmann model to obtain the corresponding admittances. Data thus obtained, with injector configuration # 2 and for the series 2 tests, are compared in Fig. 25 with the corresponding experimentally determined admittance data. An examination of this figure shows a reasonable agreement between the measured and predicted admittances. This agreement provides further support to the notion that τ_b^* is indeed frequency dependent. In addition, these data indicate that the magnitude of the characteristic combustion time can be determined with reasonable accuracy from measurements of the axial steady state temperature distribution in the vicinity of the injector. An examination of Fig. 25 also supports the conclusion, made earlier from the measured admittance data of configuration # 1, that the magnitude of the real part of the complex admittance decreases with an increase in the equivalence ratio. This implies a decrease in the maximum driving

capacity of the injector with a decrease in the amount of fuel input into the system. Also, the frequency at which this maximum amount of driving is observed decreases with an increase in the equivalence ratio.

Effect of Number of Elements on Injector Admittance

A comparison between the measured reactive admittances of injector configuration # 1 with the corresponding data of configuration # 2 is presented in Fig. 26. These data are with flow rates corresponding to series 2 of Table I and an equivalence ratio of 0.57. For comparison purposes, the nonreactive data for the above mentioned situations that were discussed in an earlier section are also presented in Fig. 26. An examination of this figure indicates that for a fixed oxidizer and fuel flow rates and a given open-area ratio the frequency range during which the reactive injector can sustain combustion instabilities depends upon the number of individual injectors. In addition, the data also indicate that at the frequency at which the negative real part of the complex admittance is maximum decreases with a decrease in the number of injector elements. At this point a reexamination of the Feiler and Heidmann predicted data, presented earlier in Figs. 1 and 21, indicates that for a given injector and flow rates an increase in the assumed τ_b^* value results in (1) a shift in the driving frequency range to a lower scale and(2) a decrease in the magnitude of the maximum driving capability and the

frequency at which this maximum driving occurs. These observations are similar to the earlier comments made by examining the data presented in Fig. 26 for the two test injectors having the same geometry and operating flow rates but differing only in the number of injector elements. This comparison, therefore, suggests that the effect of decreasing the number of elements of a given injector is to increase the characteristic combustion time τ_b^*. This supports an identical observation made independently from a comparison of the characteristic combustion times of the two injectors that were computed from temperature measurements and presented in the previous section.

Empirical Correlations of Self-Driving Periods

As a part of this investigation, a series of reactive tests were conducted wherein the oxidizer flow rate was kept fixed and the acetylene flow rates were varied to obtain test conditions having different equivalence ratios. If the system was observed to self-oscillate at each of these equivalence ratios, then the self-driving frequency of the system was noted and the half-period of the self-excitation frequency was calculated. The data thus obtained are presented in Figs. 27 and 28 for the coaxial injector configurations # 1 and # 2, respectively. In addition, the axial steady state temperature distributions in the vicinity of the injector were measured and the location of the plane of maximum steady state

temperature was determined for some of the above-mentioned tests. Following the simplistic approach, described in an earlier section of this report, a value of the characteristic combustion time τ_b^* was calculated and the data so obtained are tabulated in Table III and plotted in Figs. 27 and 28 for comparison with the measured half-period of the self-driving frequency. An examination of these data indicates that the values determined from the temperature data are of the same order of magnitude as the half-period of the observed self-driven oscillations. This suggests that, for systems with coaxial injectors and which are found to be inherently unstable, the half-periods of the observed oscillations can be used during a preliminary stability analyses to represent the characteristic combustion times. These experimental results also support the well known notion[7] that optimum conditions for instability occur when the ratio of the characteristic problem times satisfies a certain criterion.

Porous Plate Injector Admittances

The coaxial injector admittance data presented so far in this report were those of the oxidizer elements and were obtained under conditions of strong coupling between the oscillations in the oxidizer dome of the injector and the combustion chamber. In order to obtain injector admittance data while the oxidizer dome was decoupled from the chamber oscillations, injector configuration # 3 was designed using a porous plate for the oxidizer inlet. The details of this injector

has been presented earlier in Fig. 9. Since a low porocity plate was employed, a normalized pressure drop equal to 0.34 was required to maintain the needed air flow rate corresponding to that of series 2. This pressure drop across the injector plate in effect decoupled the oxidizer dome from the combustor. The reactive and nonreactive admittancs measured under these conditions are presented in Fig. 29. An examination of this figure indicates that the injector admittances are effectively independent of the frequency and are small in magnitude under both reactive and nonreactive conditions. Furthermore, the measured admittances are positive in magnitude indicating that the injector response to a chamber oscillation was that of a mild damper and no change in the damping characteristics was observed while the system operating condition was changed from a nonreactive to a reactive condition. The results of this study, therefore, suggest that the strong driving observed earlier with the coaxial injector configurations # 1 and # 2 is mainly due to a favorable injector combustor coupling in those configurations.

CONCLUSIONS

In this report, experimental data are presented describing the driving of acoustic instabilities by the combustion processes associated with gaseous propellant injectors. An examination of these data leads to the following conclusions:

(1) Under favorable conditions of injector-combustor coupling,

coaxial gaseous injectors are capable of initiating and sustaining combustion instabilities over certain frequency ranges.

(2) The frequency range over which a given coaxial injector can drive combustor oscillations and the frequency at which a maximum driving is observed depends upon the oxisdizer and the fuel flow rates and the number of individual injector elements. The magnitude of the maximum driving capability and the frequency at which this maximum occurs decreases (a) with an increase in the equivalence ratio for a given oxidizer flow rate, (b) with a decrease in the oxidizer flow rate with the equivalence ratio remaining the same and (c) with a decrease in the number of injector elements for a given open-area ratio and oxidizer and fuel flow rates.

(3) Following a relatively simple approach, quantitative data describing the characteristic combustion times of coaxial injectors have been obtained from steady state temperatures measured in the vicinity of the injector. These data demonstrate that the characteristic combustion time associated with a given injector is dependent upon the frequency and the pressure drop across the injector orifices. Furthermore, the value of τ_b^* decreases with a decrease in the number of injector elements for a given constant open-area ratio and oxidizer and fuel flow rates.

(4) For unstable systems with coaxial injectors, the half-periods of the observed oscillations can be used to represent the characteristic combustion times during a preliminary stability analysis.

(5) Finally, a comparison between the measured admittance data of coaxial injectors with those predicted by the Feiler and Heidmann analytical model shows a reasonable agreement under both reactive and nonreactive conditions.

The data presented in this report should find applications in stability considerations of gaseous propellant rocket motors and gaseous fuel fired burners.

ACKNOWLEDGEMENTS

The authors acknowledge Dr. W. A. Bell for his assistance in developing the software for the data acqusition system used during this program and Dr. M. Salikuddin for allowing the use of the computer program that computed the admittances from the measured pressure data.

REFERENCES

1. Barrere, M. and Williams, F. A., "Comparison of Combustion Instabilities Found in Various Types of Combustion Chambers," Twelfth Symposium (International) on Combustion, The Combustion Institute, 1971, pp. 169-181.

2. Feiler, C. E. and Heidmann, M. F., Dynamic Response of Gaseous Hydrogen Flow System and Its Application to High Frequency Combustion Instability, NASA TN D-4040, 1967.

3. Crocco, L. and Sirignano, W. A., Behavior of Supercritical Nozzles under Three Dimensional Oscillatory Conditions, AGGARDograph 117, Butterworths, 1967.

4. Buffum, R. G., Dehority, G. L., Slates, R., and Price, E. W., "Acoustic Attenuation Experiments on Subscale Cold Flow Rocket Motors," AIAA Journal, 5, 1967, pp. 272-280.

5. Bell, W. A., Daniel, B. R., and Zinn, B. T., "Experimental and Theoretical Determination of Admittances of a Family of Nozzles Subjected to Axial Instabilities," Journal of Sound and Vibration, 30, 1973, pp. 179-190.

6. Janardan, B. A., Daniel, B. R. and Zinn, B. T., "Damping of Axial Instabilities by Small-Scale Nozzles Under Cold-Flow Conditions," Journal of Spacecraft and Rockets, 11, 1974, pp. 812-820.

7. Harrje, D. T., Ed. Liquid Propellant Rocket Combustion Instability, NASA SP-194, 1972.

8. Priem, R. J. and Yang, J. Y. S., Technique for Predicting High Frequency Stability Characteristics of Gaseous Propellant Combustors, NASA TN D-7406, 1973.

9. Putnam, A. A., Combustion Driven Oscillations in Industry, Elsevier, 1971.

10. Schimmer, H. and Vortmeyer, D., "Acoustic Oscillation in a Combustion System with a Flat Flame," Combustion and Flame, 28, 1977, pp. 17-24.

11. Baade P. K., "Combustion Oscillations in Gas Fired Appliances," A.G.A. and I.G.T. Conference on National Gas Technology, Atlanta, 1972.

12. El Banhawy, Y., Melling, A. and Whitelow, J. H., "Combustion Driven Oscillations in a Small Tube," Combustion and Flame, 33, 1978, pp. 281-290.

13. Sipowicz, W. W., Ryan, N. W. and Baer, A. D., "Combustion Driven Acoustic Oscillations in a Gas-Fired Burner," Thirteenth Symposium (International) on Combustion, The Combustion Institute, 1971, pp. 559-564.

14. Toong, T. Y., Salant, R. F., Stopford, J. M. and Anderson, G. Y., "Mechanisms of Combustion Instability," Tenth Symposium (International) on Combustion, The Combustion Institute, 1965, pp. 1301-1313.

15. Jarosinski, J. and Wojcicki, S., "The Mechanism of Interaction between a Combustion Region and Acoustic Resonator," Acta Astronautica, 3, 1976, pp. 567-572.

16. Calhoon, D. F., Ito, J. I. and Kors, D. L., Investigation of Gaseous Propellant Combustion and Associated Injector/Chamber Design Guidelines, NASA CR-121234, 1973.

17. Williams, F. A., Combustion Theory, Addison-Wesley, 1965, p. 222.

18. Janardan, B. A., Daniel, B. R., and Zinn, B. T., Characteristics of Response Factors of Coaxial Gaseous Rocket Injectors, NASA CR-134788, 1975.

19. Crocco, L., Grey, J. and Mathews, G. B., "Preliminary Measurements of the Combustion Time Lag in a Monopropellant Rocket Motor," Fifth Symposium (International) on Combustion, The Combustion Institute, 1954, pp. 164-170.

20. Baev, V. K. and Tret'yakov, P. K., "Characteristic Burning Times of Fuel-Air Mixtures," Combustion, Explosion and Shock Waves, 4, 1969, pp. 208-214; translated from Fizika Goreniya i Vzryva, 4, 1968, pp. 367-376.

21. Kapur, A., Cummings, A. and Mungur, P., "Sound Propagation in a Combustion Can with Axial Temperature and Density Gradients," Journal of Sound and Vibration, 25, 1972, pp. 129-138.

22. Cummings, A., "Sound Generaion and Transmission in Flow Ducts with Axial Temperature Gradienst," Journal of Sound and Vibration, 57, 1978, pp. 261-279.

23. Salikuddin, M. and Zinn, B. T., "Adaptation of the Impedance Tube Technique for the Measurement of Combustion Process Admittances," 17th Aerospace Sciences Meeting, New Orleans, AIAA Paper No. 79-0167, 1979.

24. Repas, G. A., "Rocket Propellant Injection," Patent, NASA-Case-Lewis-1107-1, 1973.

Table I. Operating Flow Rates

FUEL	FLOW SERIES	$\dot{W}^*_{ox}$	$\dot{W}^*_f$	q
Acetylene	1	0.78	0.103	0.57
			0.058	1.02
			0.045	1.31
			0.000	NR
	2	1.56	0.206	0.57
			0.115	1.02
			0.090	1.31
			0.000	NR
	3	3.12	0.412	0.57
			0.230	1.02
			0.180	1.31
			0.000	NR
Methane	4	0.4	0.047	0.495
			0.024	0.97
			0.000	NR

Table II. Test Matrix

Injector Configuration	# 1			# 2			# 3
Flow Series	1	2	3	1	2	3	2
Eq. Ratio (Fuel-Acetylene)							
0.57	x	x		x	x	x	x
1.02		x		x	x	x	x
1.31		x		x	x	x	x
NR	x	x	x	x	x	x	x

Flow Series	4
Eq. Ratio (Fuel-Methane)	
0.50	x
0.97	x
NR	x

Table III. Self-Driving Test Results

Injector Configuration	Oxidizer Flow Rate	Eq. Ratio	½ period at Self-Driving Frequency msec	τ_b^* From Temperature Data msec
# 1	Series 2	0.45	0.67	0.49
		0.49	0.67	0.49
		0.55	0.66	0.51
		0.57	0.69	0.59
		0.57	0.69	0.68
		0.57	0.67	0.71
		0.69	0.66	0.54
		0.85	0.64	0.49
		0.95	0.64	0.49
		1.02	0.78	0.67
		1.31	0.73	1.00
	Series 1	0.57	0.81	1.10
# 2	Series 2	0.57	1.46	1.23
		0.57	1.49	1.23
	Series 3	0.57	0.91	0.83
		0.57	0.91	0.82
		1.02	0.70	0.71
		1.08	0.73	0.54
		1.15	0.73	0.55
		1.16	0.72	0.59
		1.40	0.99	0.76

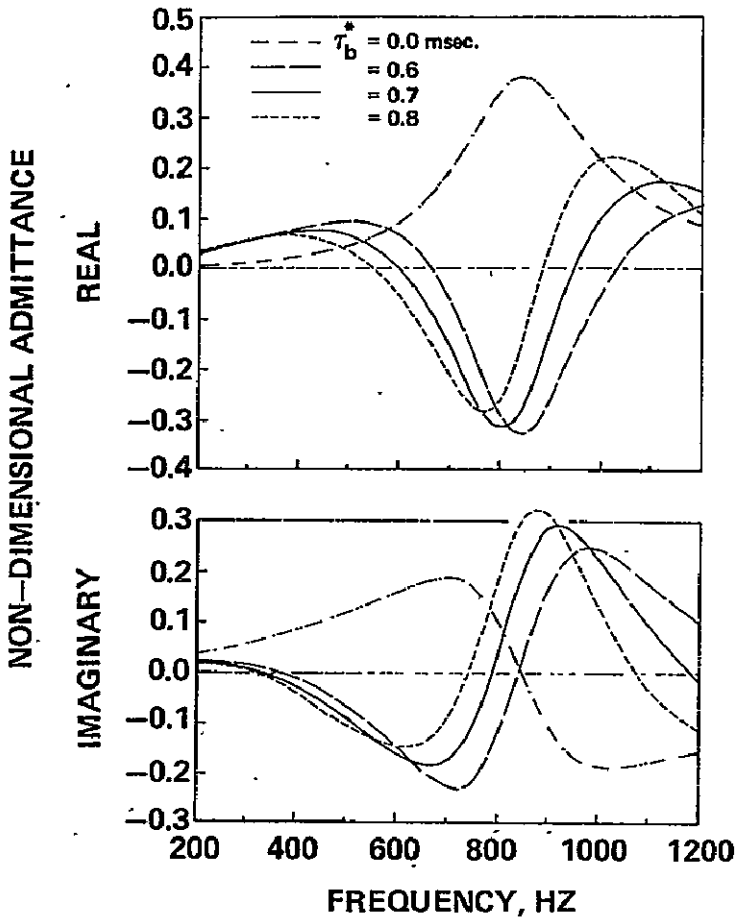

Figure 1. Effect of Characteristic Combustion Time Upon the Feiler and Heidmann Predicted Admittances.

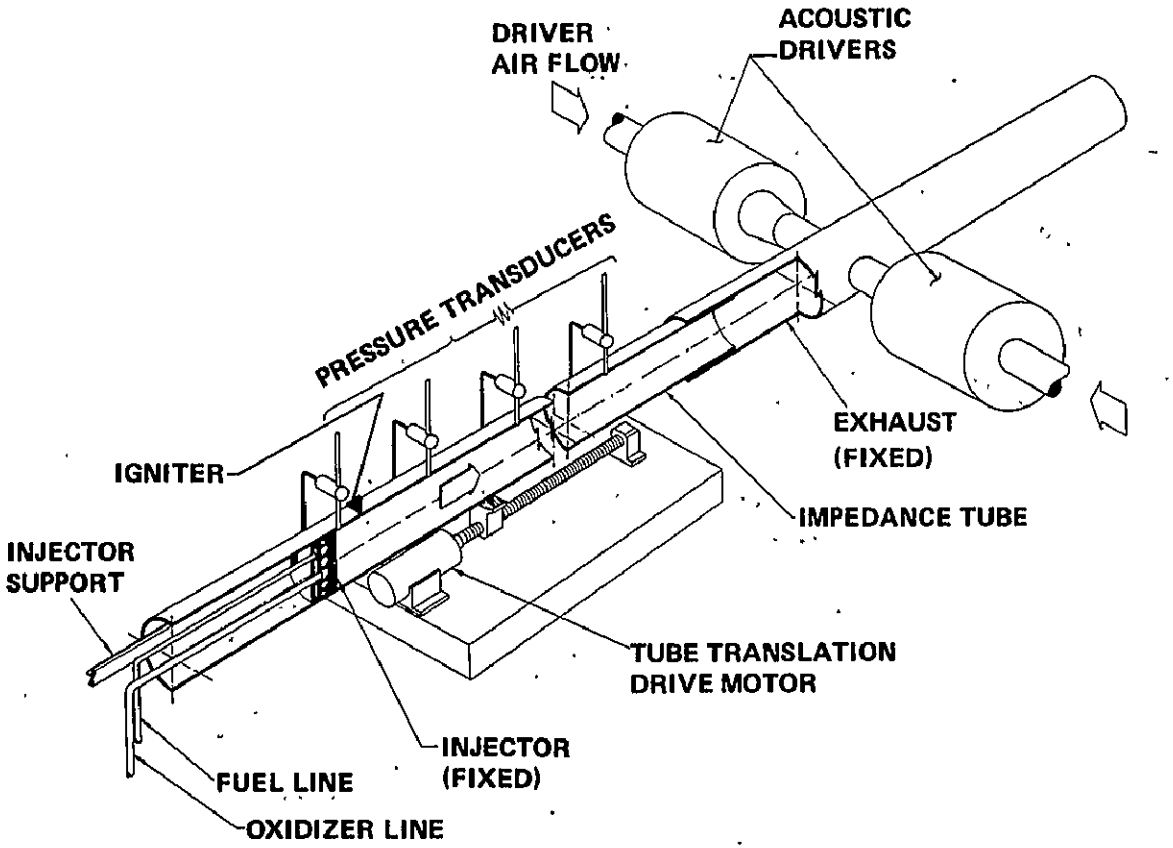

Figure 2. Sectional View of the Test Apparatus.

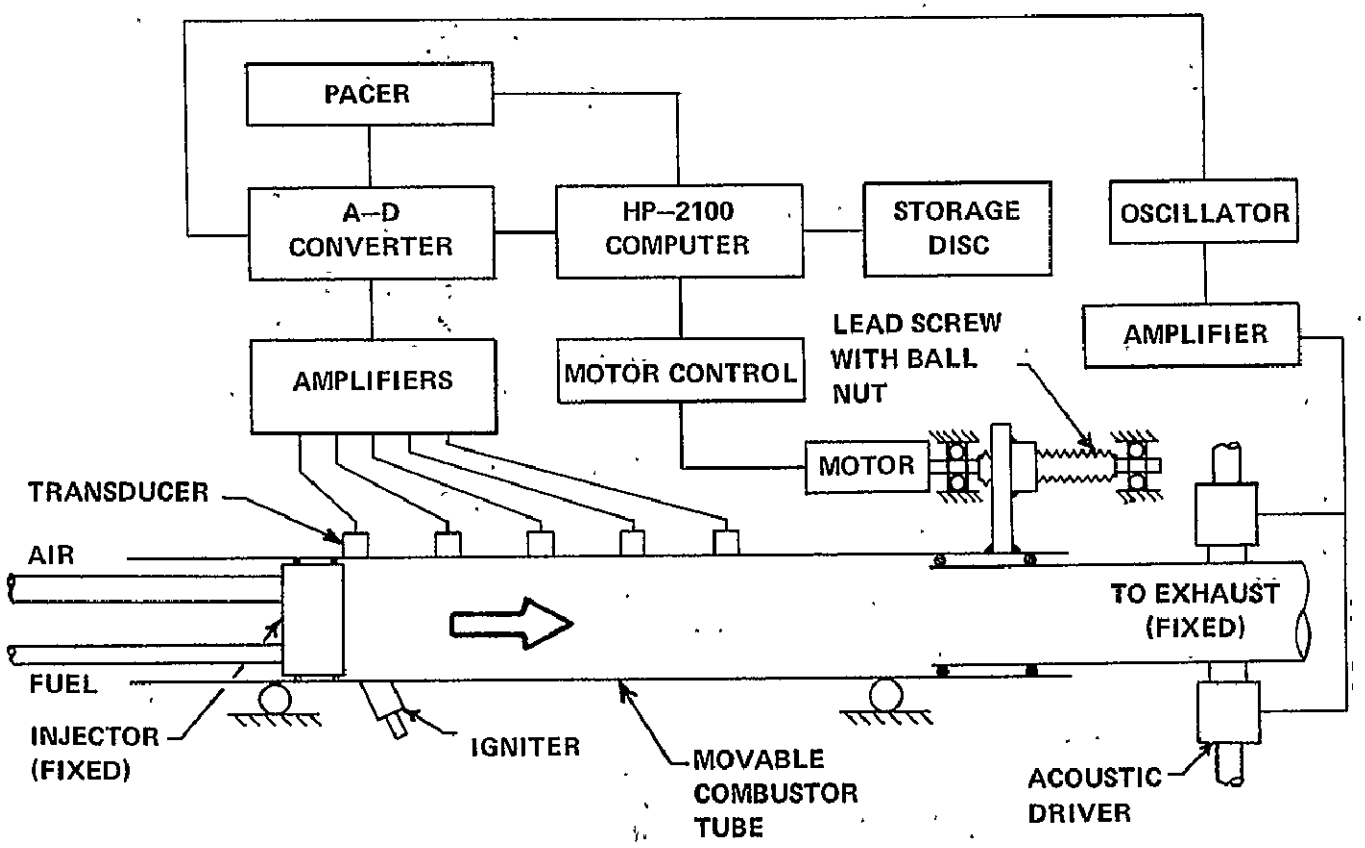

Figure 3. Instrumentation System.

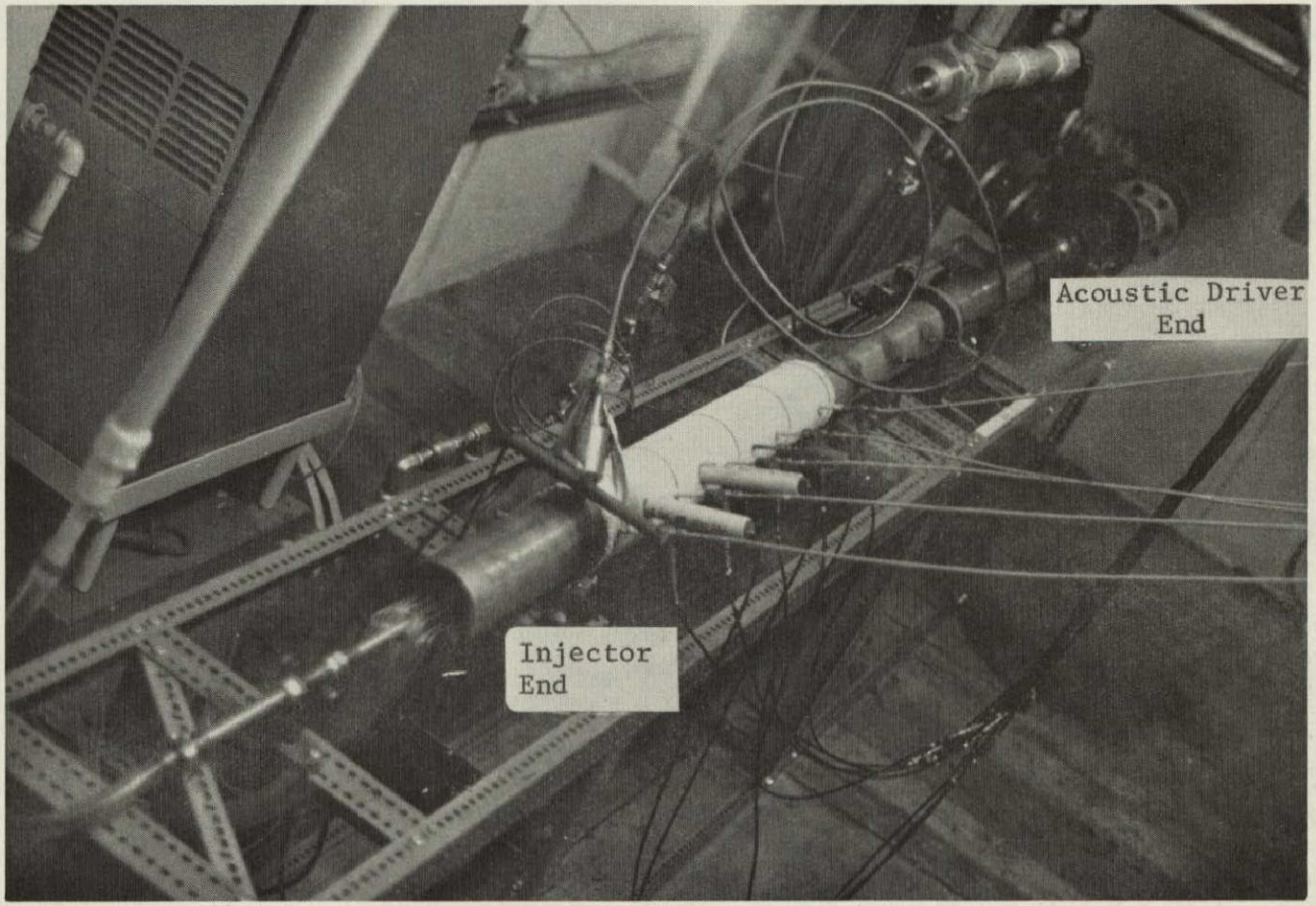

Figure 4. Pictorial View of the Experimental Apparatus.

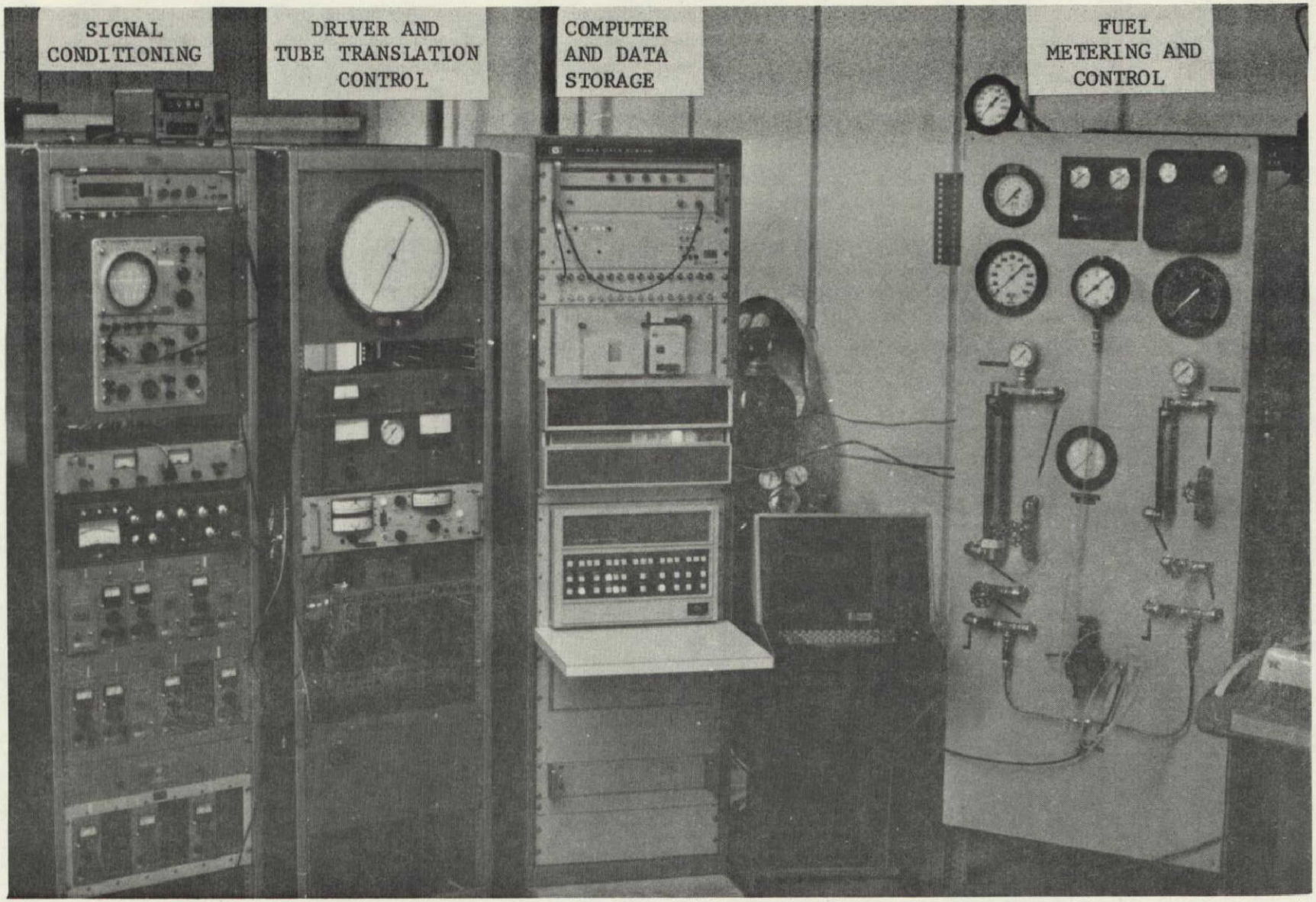

Figure 5. Experiment Control Area.

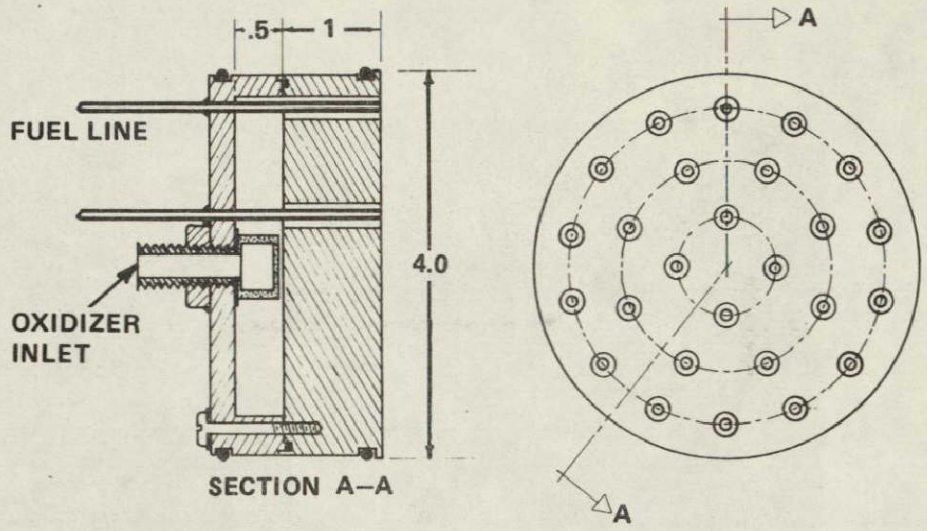

Figure 6. Coaxial Injector: Configuration # 1
(26 Injector Elements).

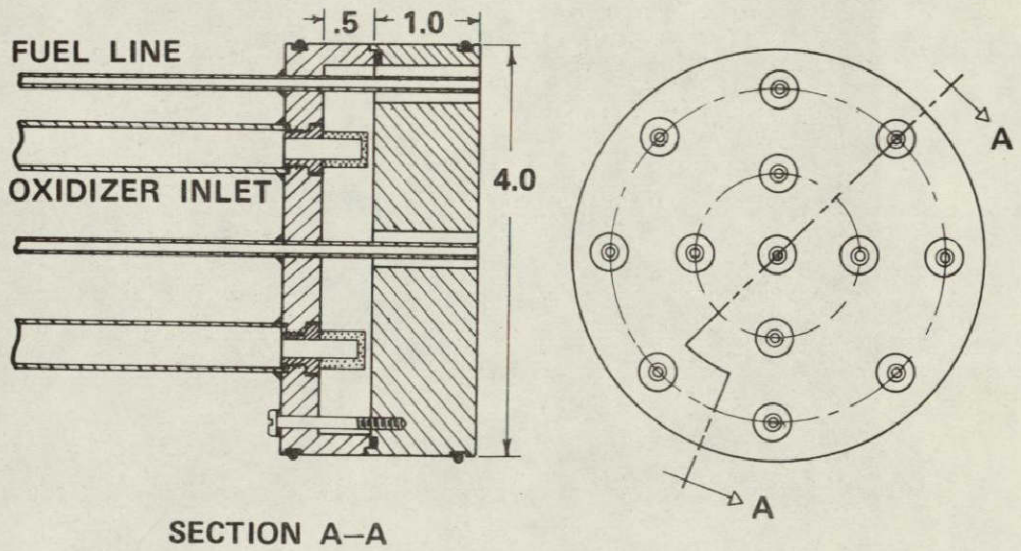

Figure 7. Coaxial Injector: Configuration # 2
(13 Injector Elements).

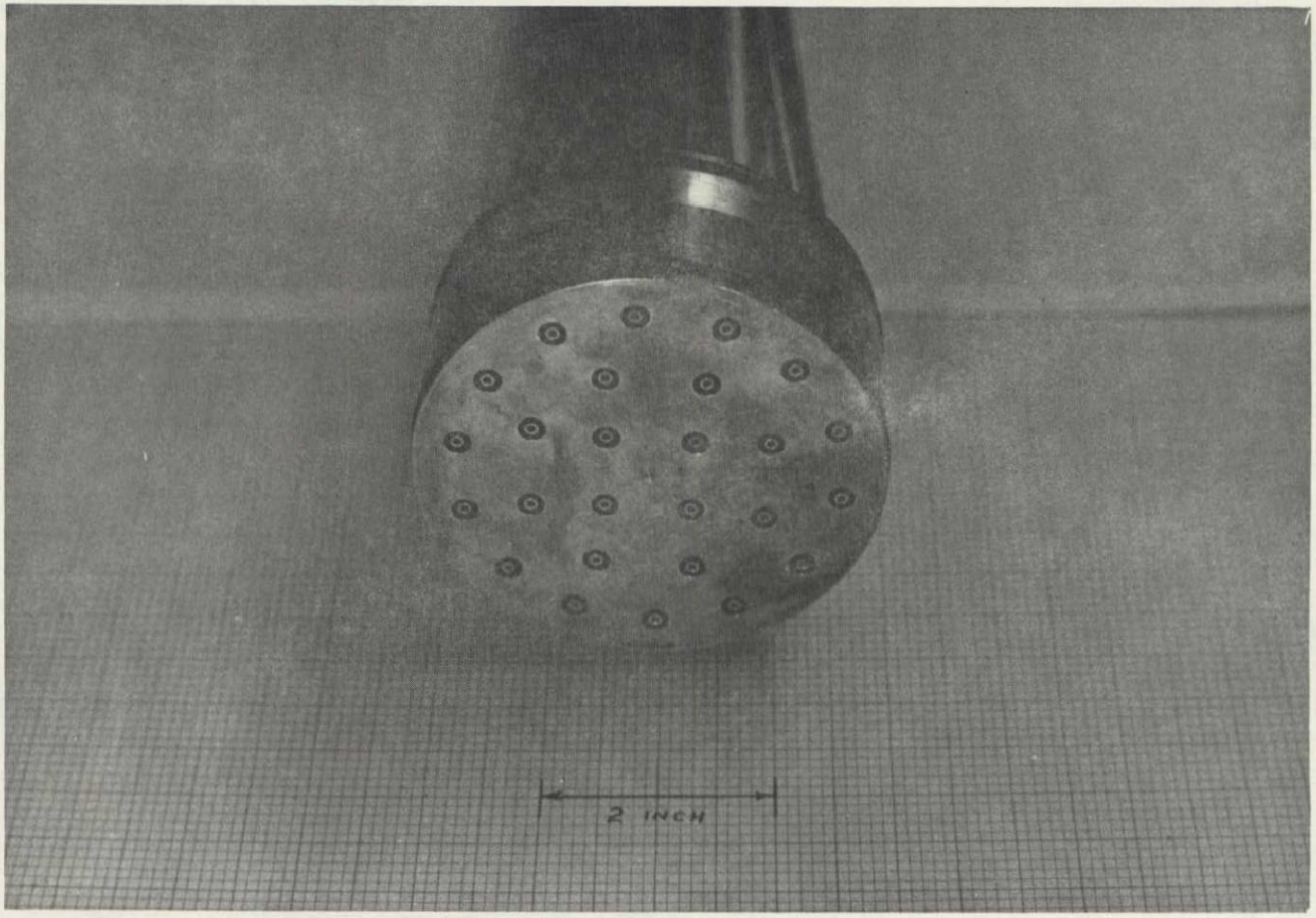

Figure 8. Pictorial View of Coaxial Injector Configuration # 1.

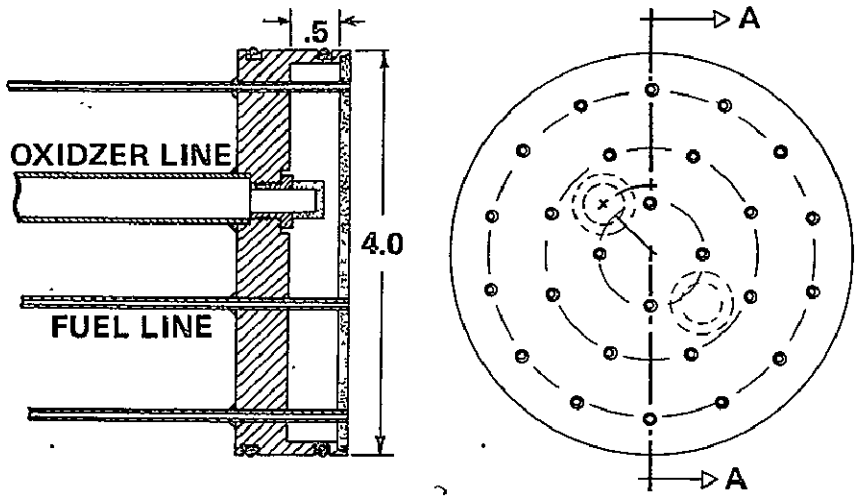

Figure 9. Porous Plate Injector: Configuration # 3.

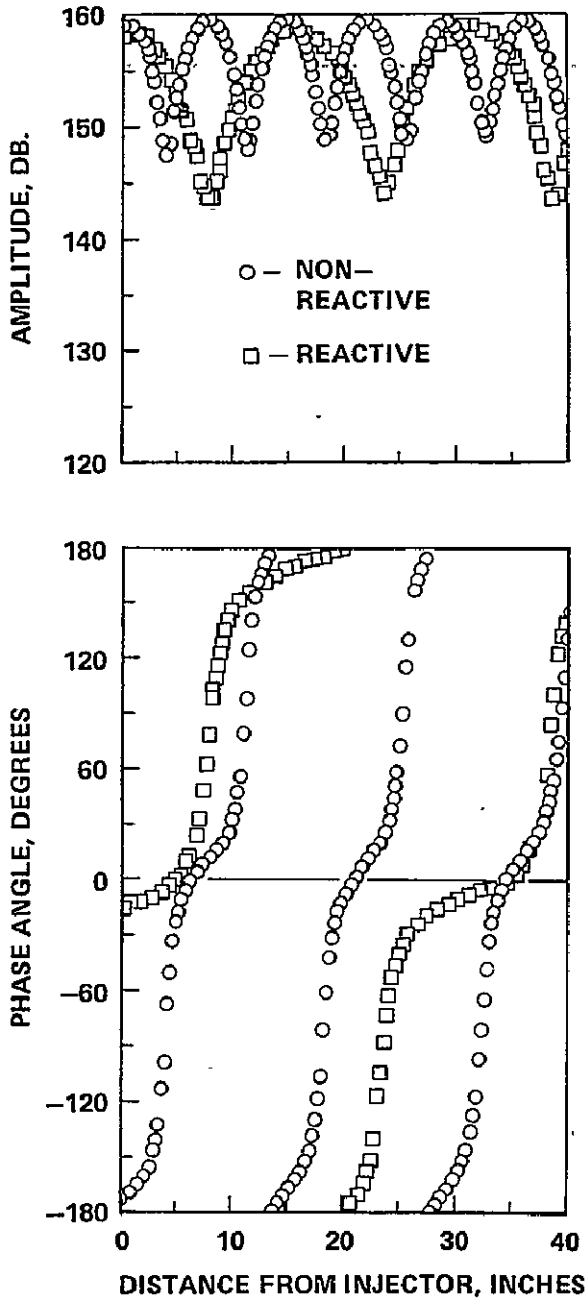

Figure 10. Axial Dependence of Pressure Amplitude and Phase: Coaxial Injector Configuration # 1, Flow Series 2, Equivalence Ratio = 1.31; Driver Frequency= 954 Hz.

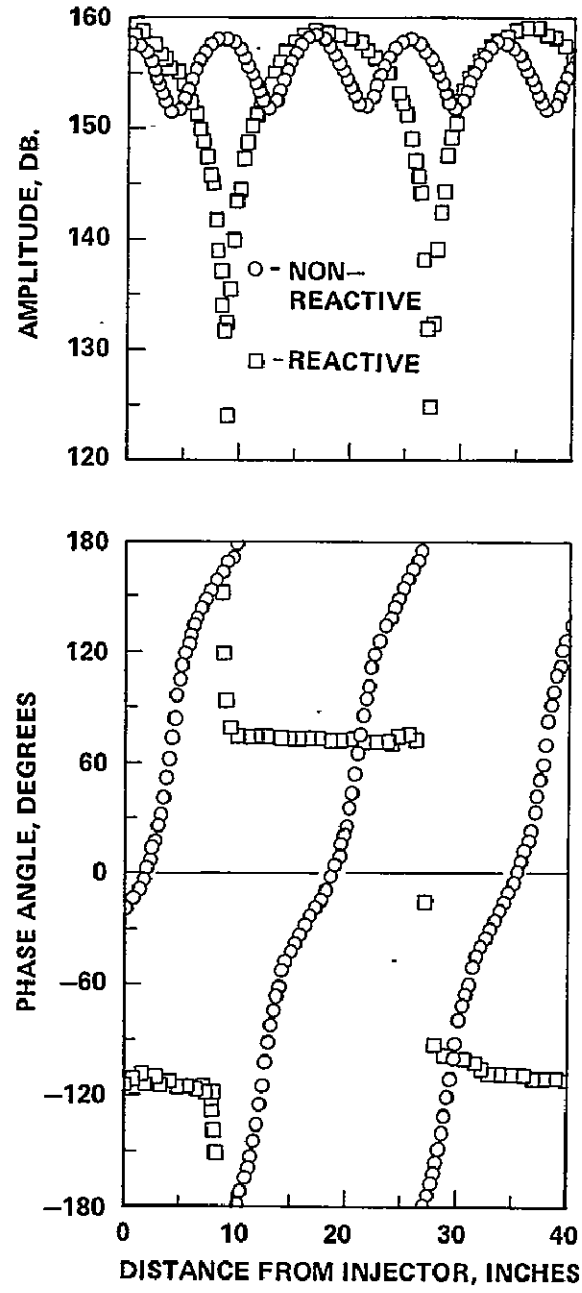

Figure 11. Axial Dependence of Pressure Amplitude and Phase: Coaxial Injector Configuration # 1, Flow Series 2, Equivalence Ratio = 1.31; Driver Frequency = 805 Hz.

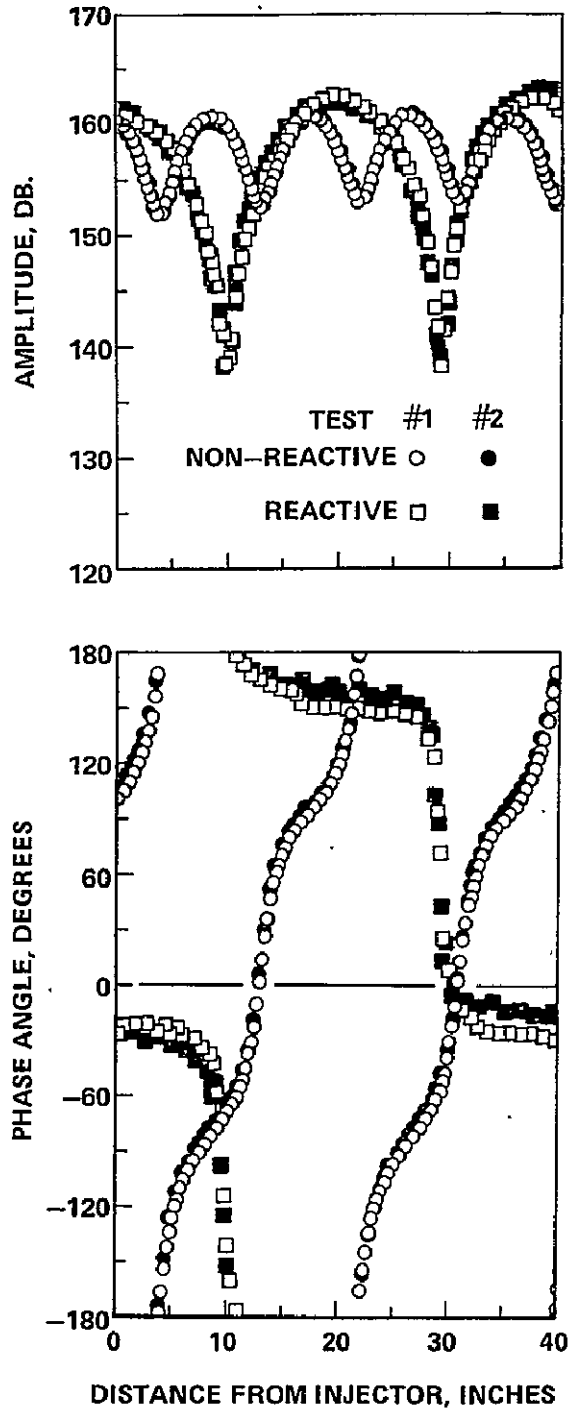

Figure 12. Axial Dependence of Pressure Amplitude and Phase: Coaxial Injector Configuratin # 1, Flow Series 2, Equivalence Ratio = 1.31; Driver Frequency = 750 Hz.

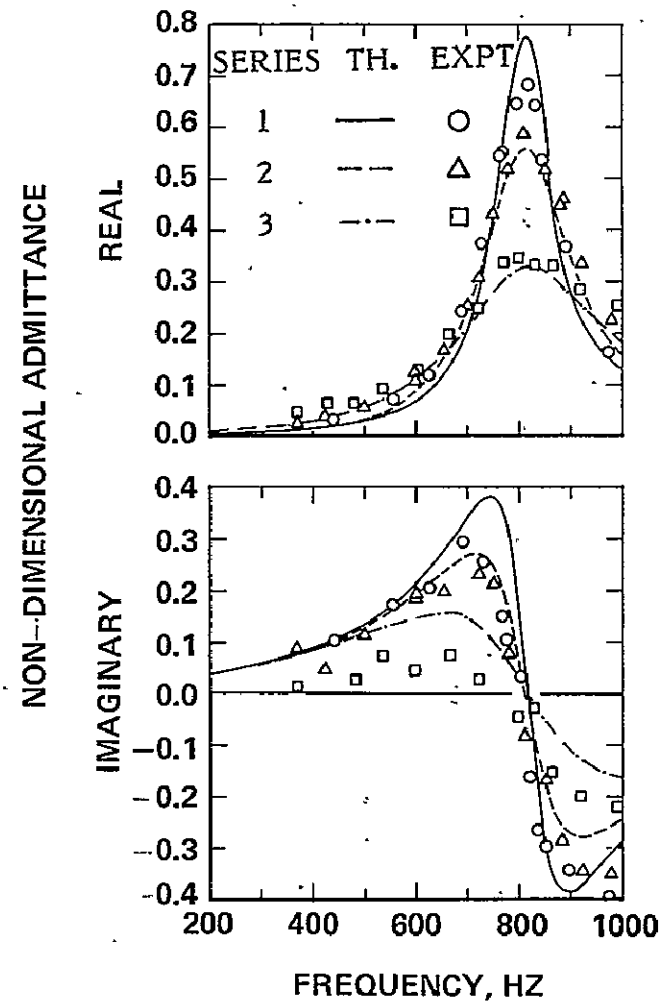

Figure 13. Dependence of Non-Reactive Admittances of Coaxial Injector Configuration # 2 upon Propellant Flow Rates.

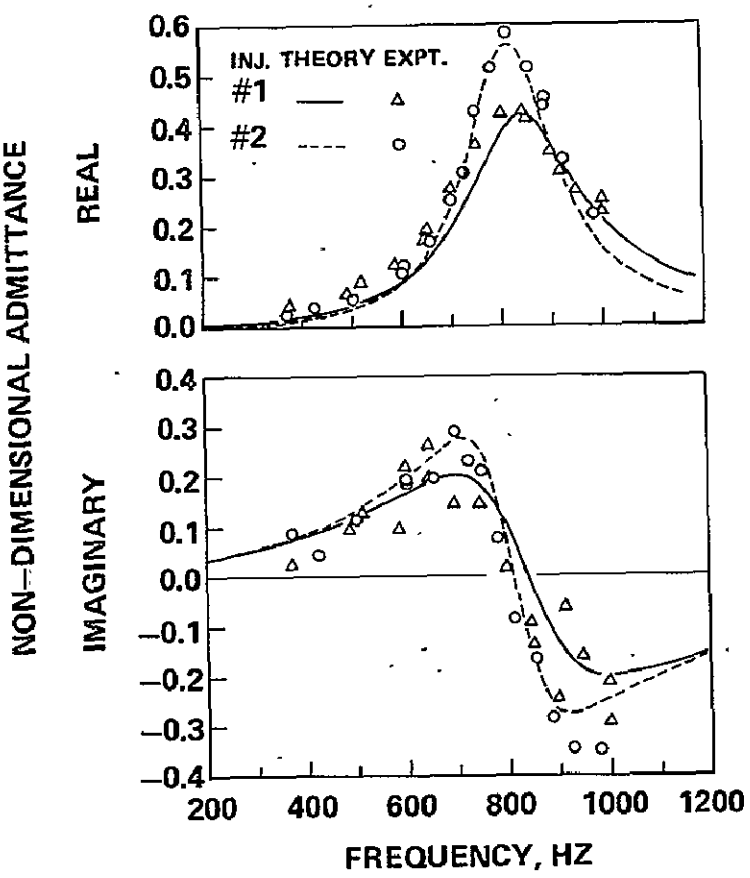

Figure 14. Effect of Number of Elements in Coaxial Injectors upon Non-Reactive Admittances: Flow Series 2.

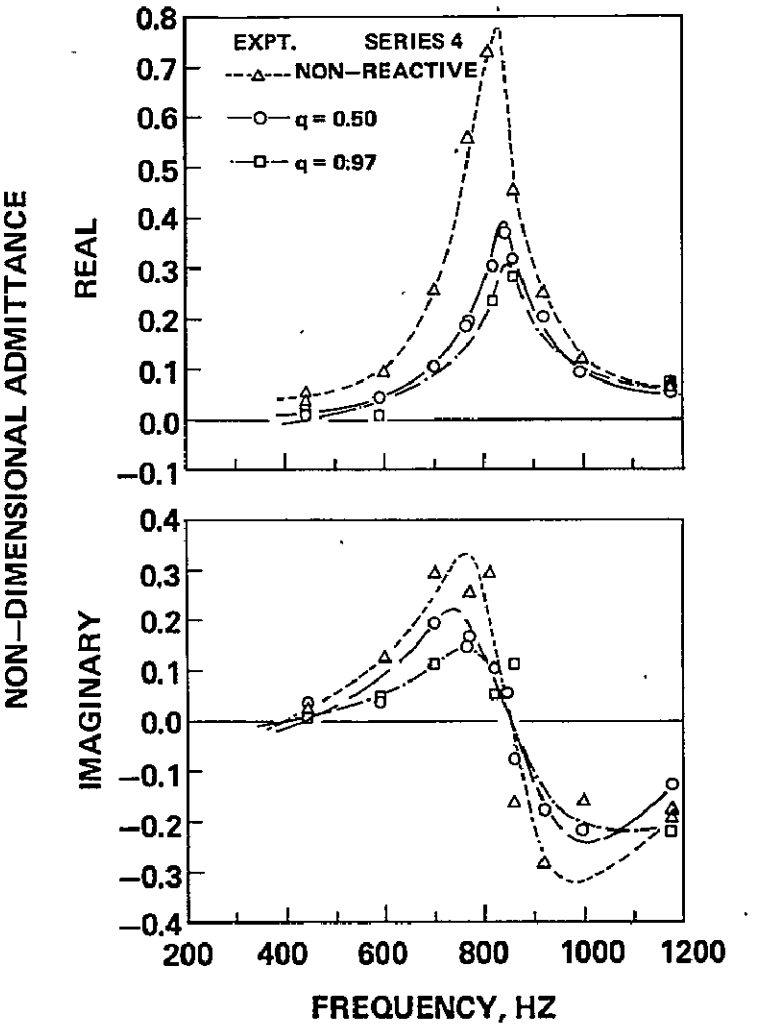

Figure 15. Comparison of Measured Non-Reactive and Reactive Admittances of Coaxial Injector Configuration # 1: Fuel-Methane, Flow Series 4.

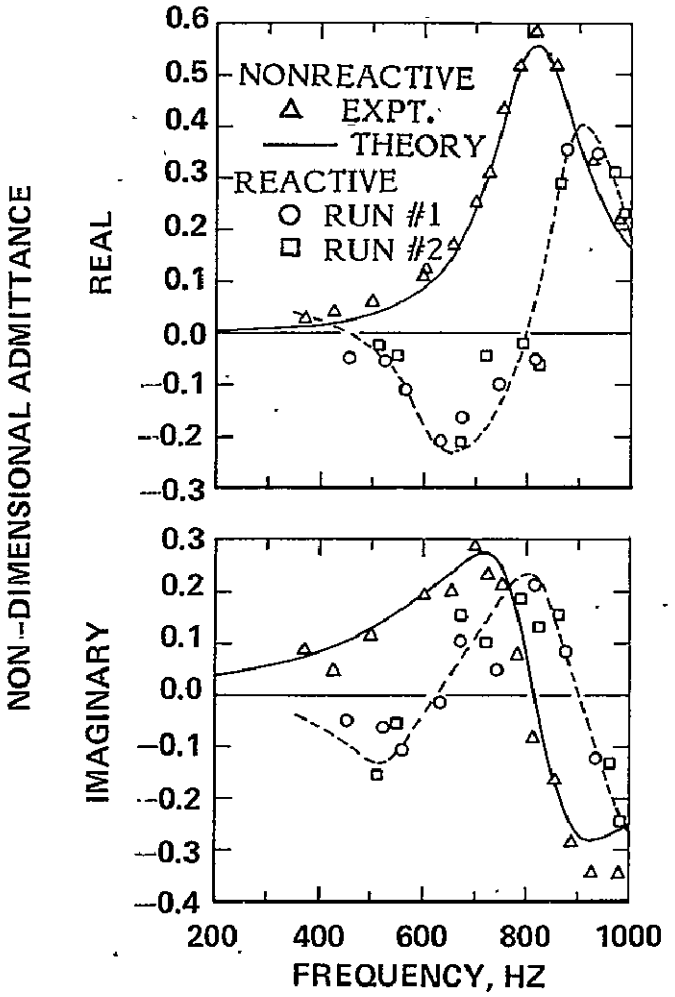

Figure 16. Comparison of Measured Reactive with Non-Reactive Admittances of Coaxial Injector Configuration # 2: Flow Series 2, Equivalence Ratio = 0.57.

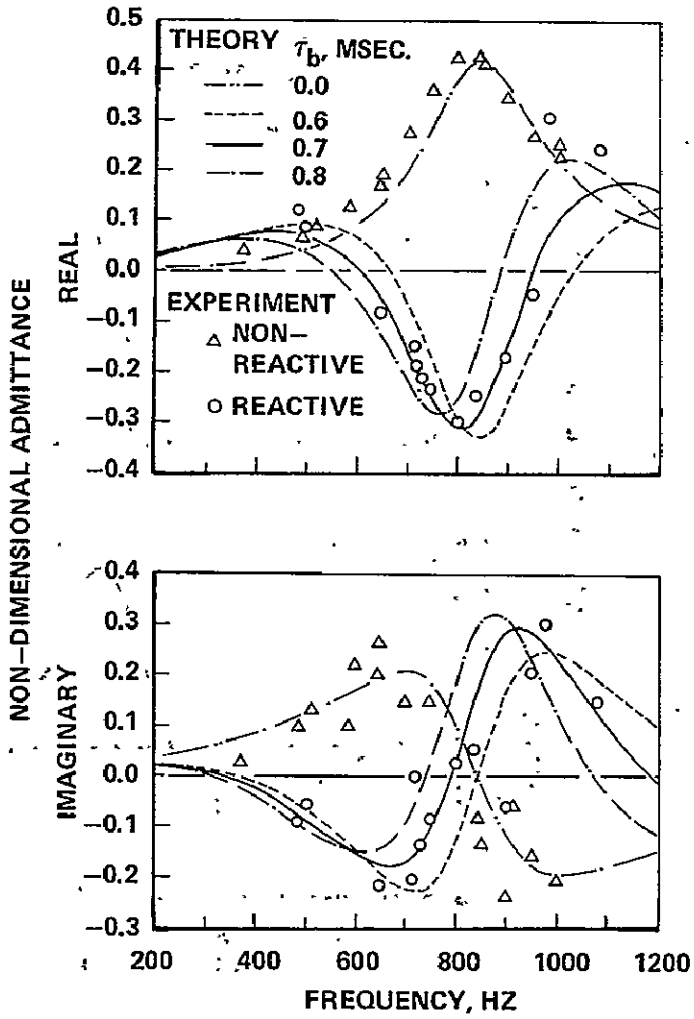

Figure 17, Comparison of Reactive with Non-Reactive Admittances of Coaxial Injector Configuration # 1: Flow Series 2, Equivalence Ratio = 0.57.

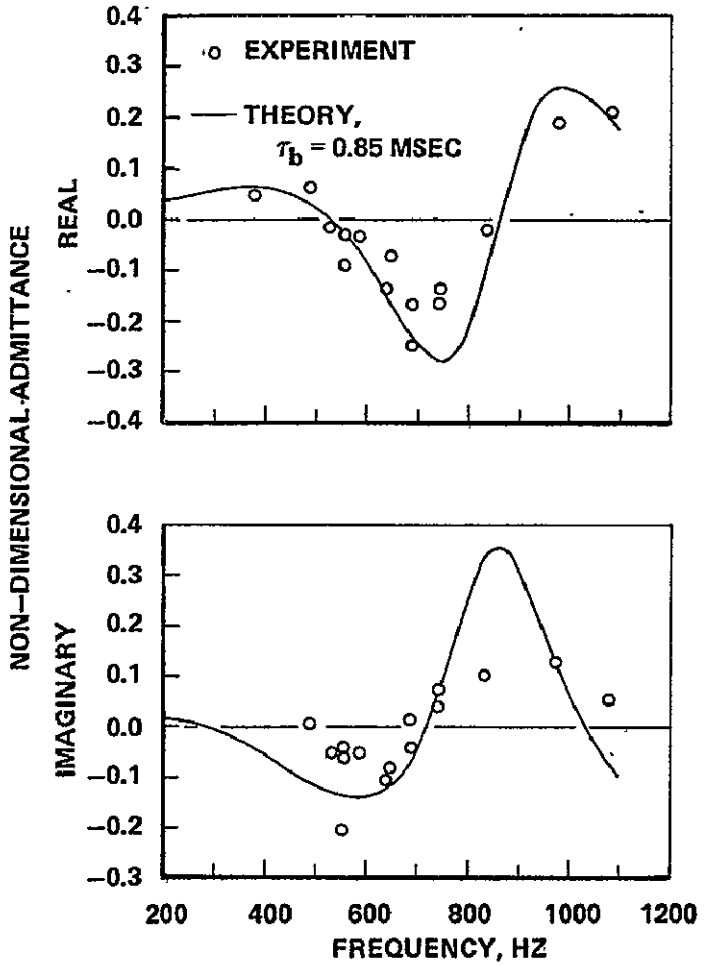

Figure 18. Frequency Dependence of Reactive Admittance of Coaxial Injector Configuration # 1; Flow Series 2, Equivalence Ratio = 1.02.

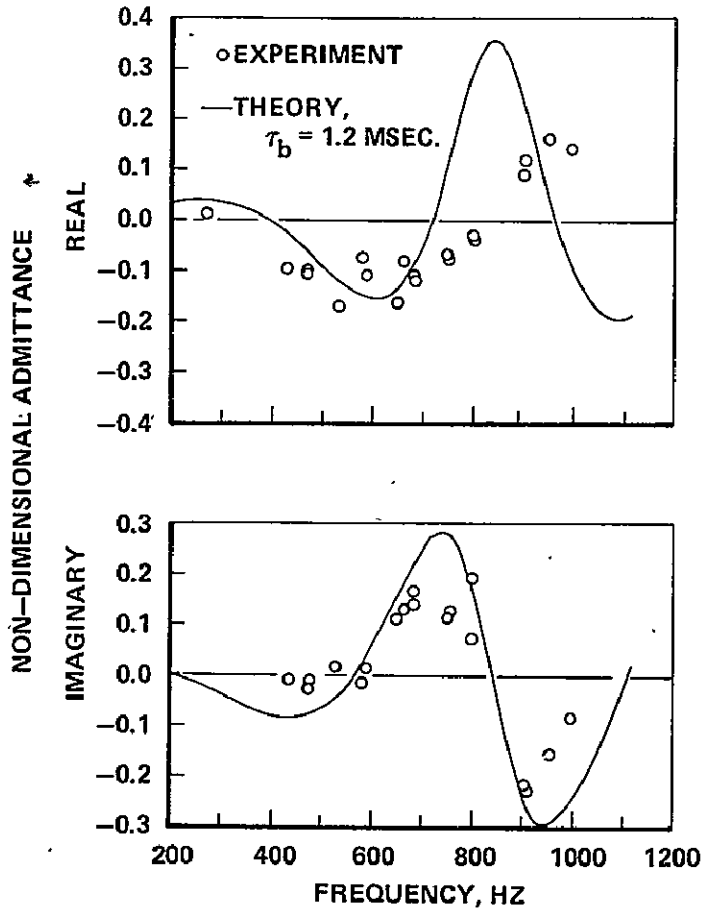

Figure 19. Frequency Dependence of Reactive Admittance of Coaxial Injector Configuration # 1: Flow Series 2, Equivalence Ratio = 1.31.

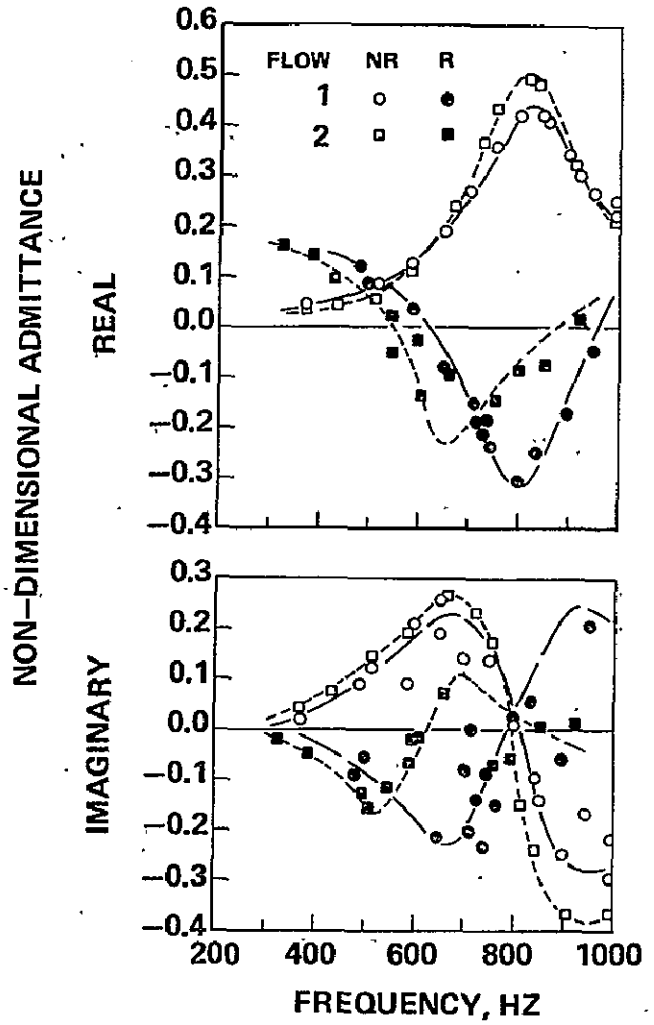

Figure 20. Dependence of Measured Admittances of Coaxial Injector Configuration # 1 upon Propellant Flow Rates: Equivalence Ratio = 0.57.

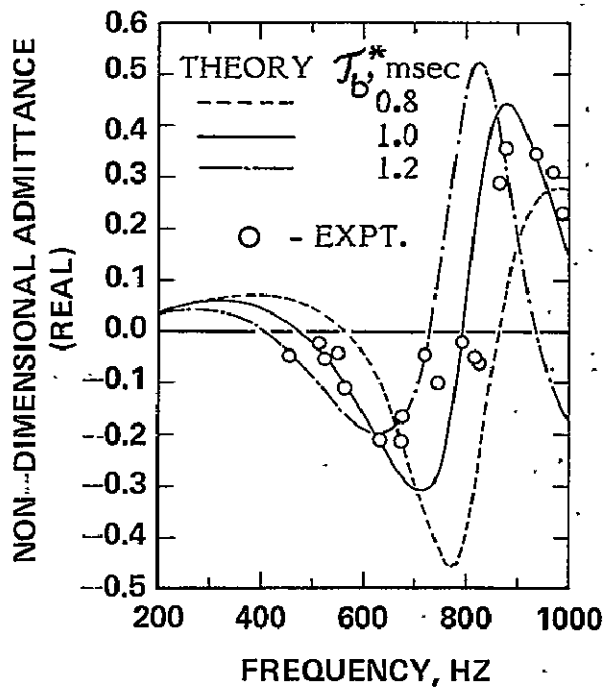

Figure 21. Comparison Between Measured and Predicted Reactive Admittances of Coaxial Injector Configuration # 2: Flow Series 2 , Equivalence Ratio = 0.57.

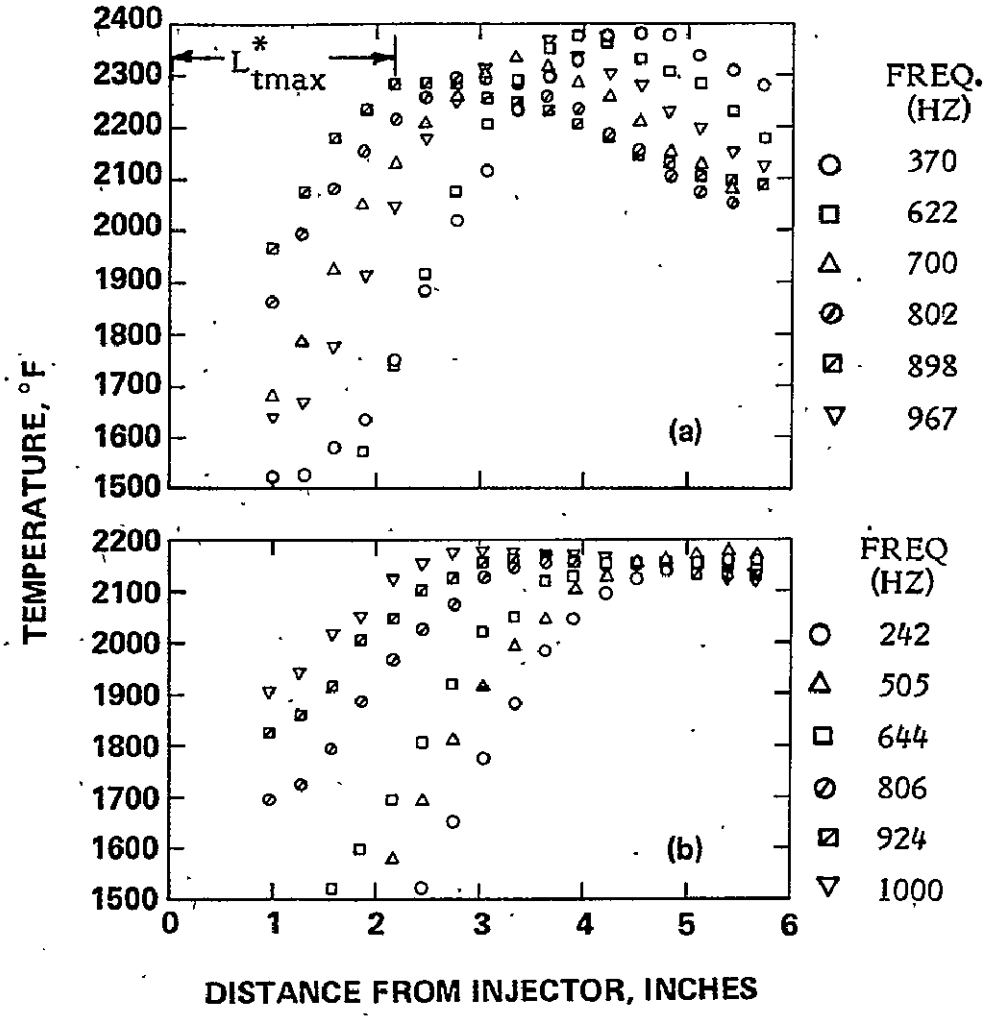

Figure 22. Measured Steady State Coaxial Temperature Distributions in the Vicinity of Injector Configuration # 2 at Different Test Frequencies, Flow Series 1: (1) Equivalence Ratio = 0.57, (b) Equivalence Ratio = 1.02.

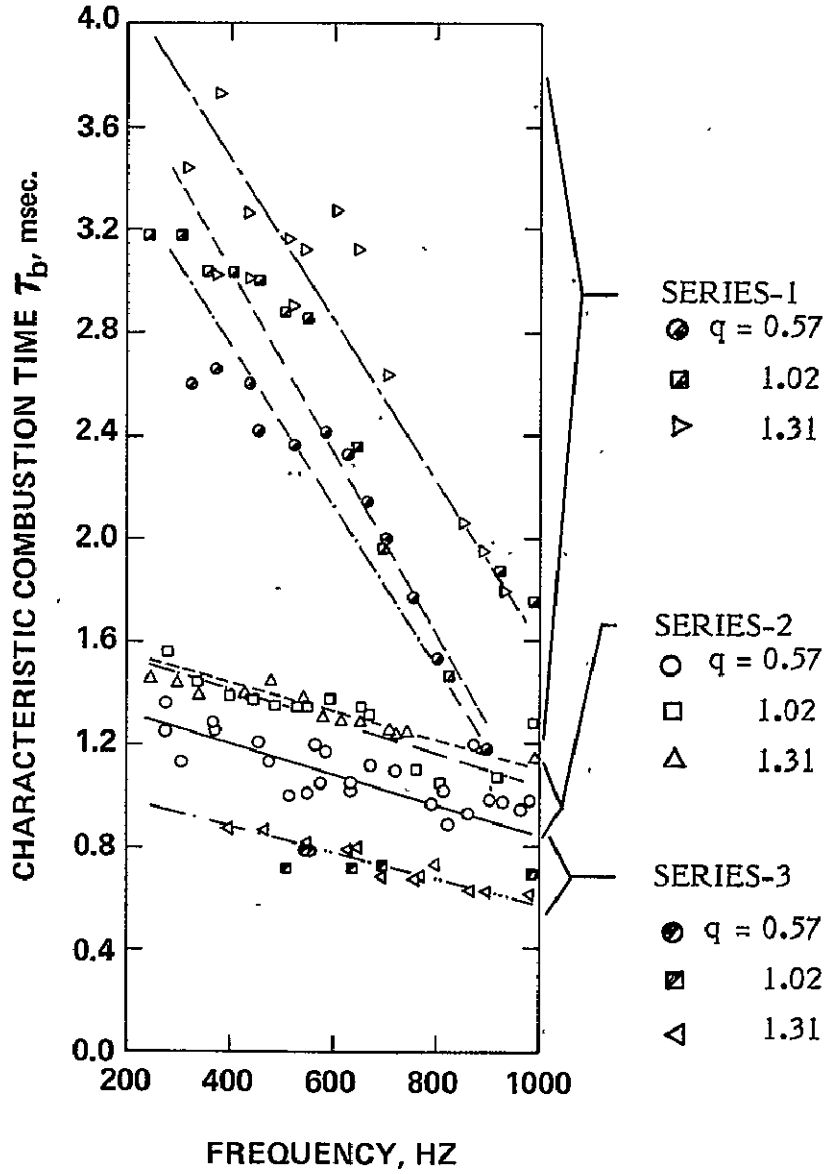

Figure 23. Frequency Dependence of the Characteristic Combustion Time of Coaxial Injector Configuration # 2 Obtained From Steady State Temperature Measurements.

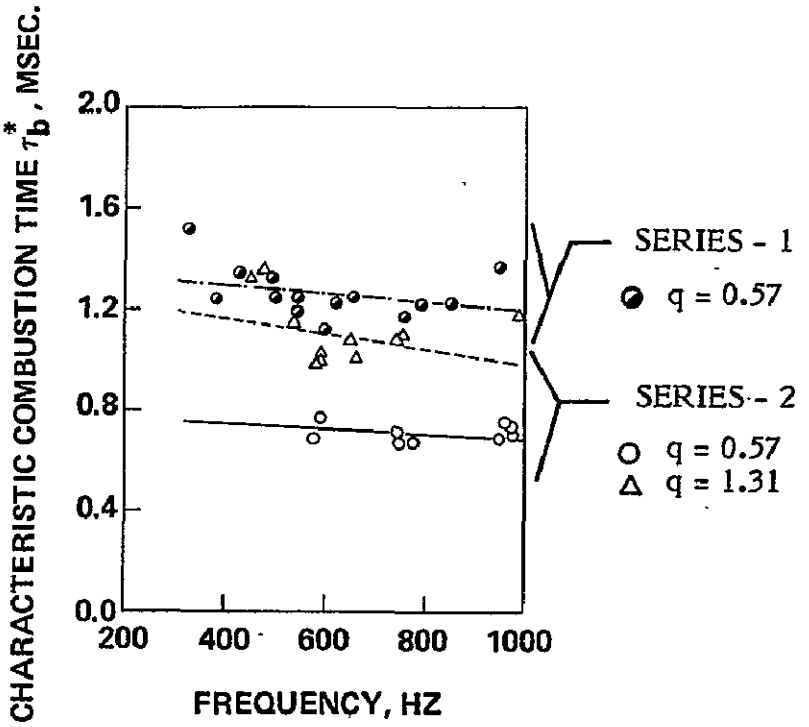

Figure 24. Frequency Dependence of the Characteristic Combustion Time of Coaxial Injector Configuration # 1 obtained From Steady State Temperature Measurements.

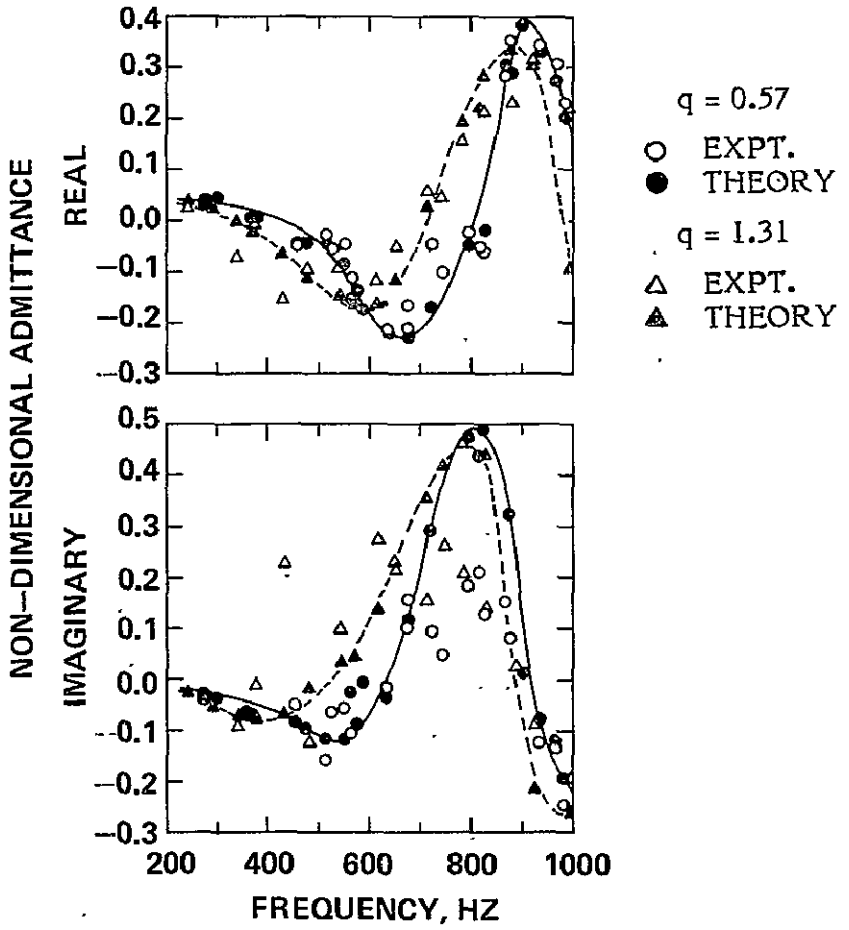

Figure 25. Comparison Between Measured Reactive Admittances of Coaxial Injector Configuration # 2 with Predicted Reactive Admittances Obtained with τ_b^* that is Calculated from Temperature Data: Flow Series 2.

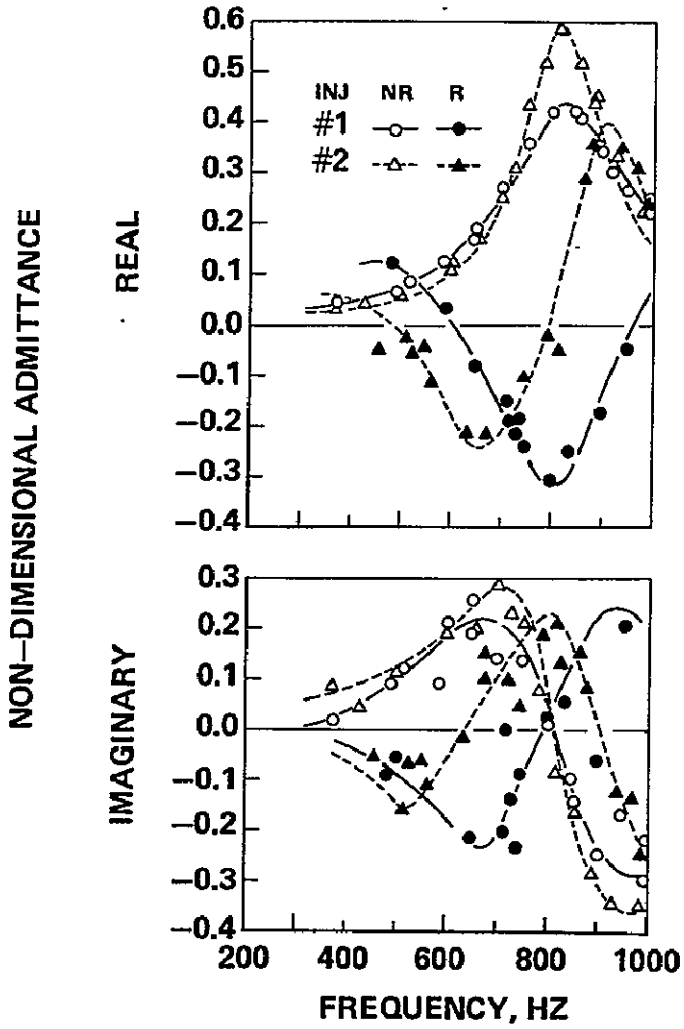

Figure 26. Effect of Number of Elements in Coaxial Injectors Upon Measured Reactive Admittances: Flow Series 2, Equivalence Ratio = 0.57.

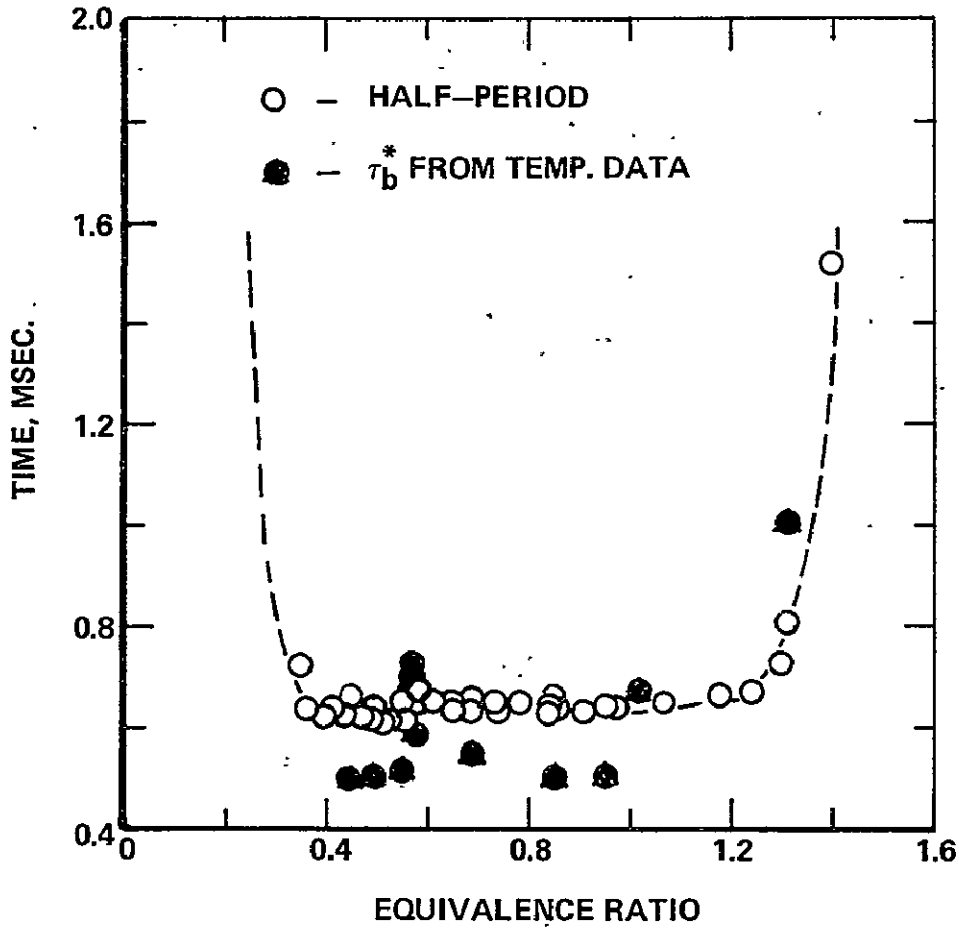

Figure 27. Dependence of Self-Excitation Half-Period of Coaxial Injector Configuration # 1 Upon Equivalence Ratio: Oxidizer Flow of Series 2.

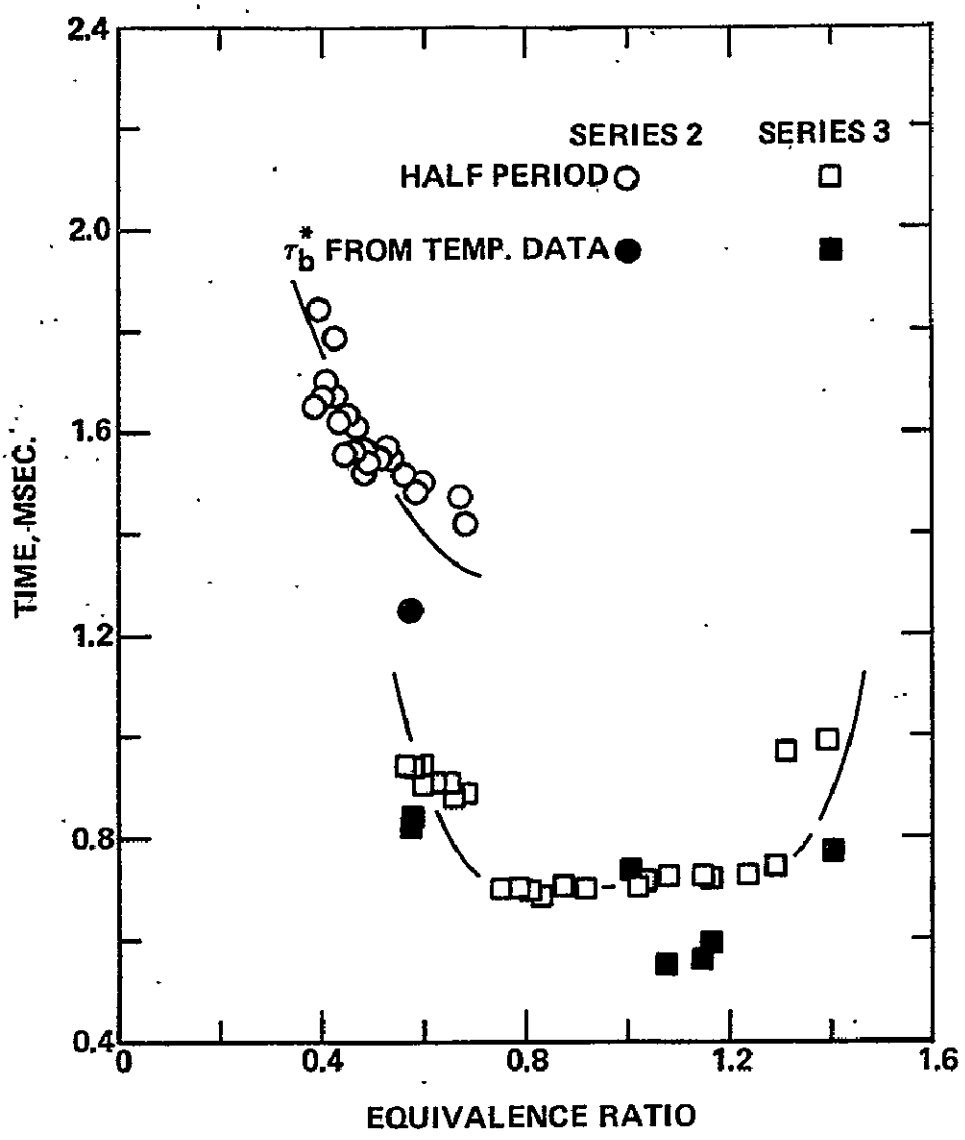

Figure 28. Dependence of Self-Excitation Half-Period of Coaxial Injector Configuration # 2 Upon Equivalence Ratio: Oxidizer Flow of Series 2 ad 3.

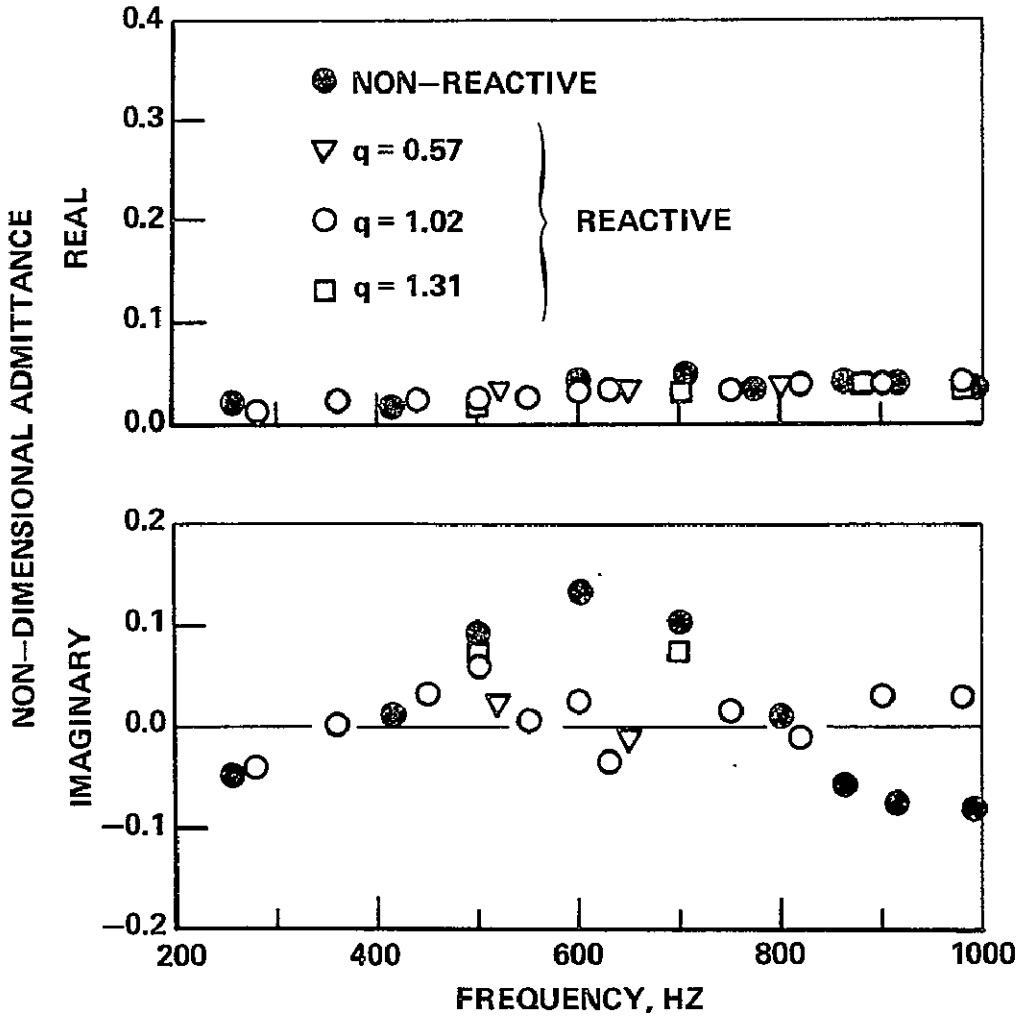

Figure 29. Measured Admittance Data of Injector Configuration # 3: Flow Series 2.

REPORT DISTRIBUTION LIST

NASA-Lewis Research Center
Attn: Dr. R. J. Priem/MS 500-204
21000 Brookpark Road
Cleveland, OH 44135
(7 copies)

NASA-Lewis Research Center
Attn: Library/MS 60-3
21000 Brookpark Road
Cleveland, OH 44135

NASA-Lewis Research Center
Attn: Report Control Office/MS 5-5
21000 Brookpark Road
Cleveland, OH 44135

NASA-Lewis Research Center
Attn: E. A. Bourke/MS 500-205
21000 Brookpark Road
Cleveland, OH 44135

NASA Headquarters
Attn: RPS/Robert A. Wasel
600 Independence Ave., SW, Rm 526
Washington, DC 20546

NASA-Lewis Research Center
Attn: 1442/Procurement Officer
Mail Stop 500-313
21000 Brookpark Road
Cleveland, OH 44135

NASA-Lyndon B. Johnson Space Center
Attn: EP/Joseph G. Thibodaux
Houston, TX 77058

NASA-George C. Marshall Space
Flight Center
Attn: S&E-ASTN-PP/R. J. Richmond
Huntsville, AL 35812

Aerojet Liquid Rocket Company
Attn: David A. Fairchild
Bldg. 20001/Sec. 9732
P. O. Box 13222
Sacramento, CA 95813

Aerojet General Corporation
Propulsion Division
Attn: R. Stiff
P. O. Box 15847
Sacramento, CA 95803

Aerospace Corporation
Attn: O. W. Dykema
P. O. Box 92957
Los Angeles, CA 90045

Aerospace Corporation
Attn: Library-Documents
2400 E. El Segundo Boulevard
Los Angeles, CA 90045

Air Force Rocket Propulsion
Lab. (RPM)
Attn. Library
Edwards, CA 93523

Air Force Office of Scientific
Research
Chief Propulsion Division
Attn: Dr. J. F. Masi (NAE)
1400 Wilson Boulevard
Arlington, VA 22209

Air Force Rocket Propulsion Lab.
Attn: Daweel George
Edwards, CA 93523

AFAPL
Research & Technology Division
AF Systems Command
U. S. Air Force
Attn: Library/APRP
Wright Patterson AFB, OH 45433

NASA Scientific & Technical Information Facility - Acquisitions Br.
P. O. Box 33
College Park, MD 20740 (10 copies)

Army Ballistics Research Labs.
Attn: Austin W. Barrows
Code AMXBR-1B
Aberdeen Proving Grounds, MD 21005

Army Ballistic Research Labs.
Attn: Ingo W. May
Code AMXBR-1B
Aberdeen Proving Grounds, MD 21005

Army Material Command
Missile Systems Div.
Attn: Stephen R. Matos
Code AMCRD-MT
5001 Eisenhower Ave.
Alexandria, VA 22304

Air Force Systems Command
Arnold Engineering Development Center
Attn: Dr. H. K. Doetsch
Tullahoma, TN 37389

Aeronutronic Div. of Philco Ford Corporation
Technical Information Dept.
Ford Road
Newport Beach, CA 92663

Battelle Memorial Institute
Attn: Report Library, Room 6A
505 King Avenue
Columbus, OH 43201

Bell Aerosystems, Inc.
Attn: Library
Box 1
Buffalo, NY 14205

Bell Aerospace Company
Attn: T. F. Ferger
P. O. Box 1
Mail Zone, J-81
Buffalo, NY 14205

Air Force Rocket Propulsion Lab
Attn: Richard R. Weiss
Edwards, CA 93523

AFAPL
Attn: Frank D. Stull (RJT)
Wright Patterson AFB, OH 45433

California Institute of Technology
Jet Propulsion Laboratory
Attn: Fred E. C. Culick
4800 Oak Grove Drive
Pasadena, CA 91103

California Institute of Technology
Jet Propulsion Laboratory
Attn: Jack H. Rupe
4800 Oak Grove Drive
Pasadena, CA 91103

California State University
Sacramento School of Engineering
Attn: Frederick H. Reardon
6000 J. Street
Sacramento, CA 95819

Chemical Propulsion Information Agency
Johns Hopkins University/APL
Attn: T. W. Christian
8621 Georgia Avenue
Silver Spring, MD 20910

Colorado State University
Attn: Charles E. Mitchell
Fort Collins, CO 80521

Frankford Arsenal
Attn: Martin Visnov
NDP-R, Bldg. 64-2
Bridge & Tacony Streets
Philadelphia, PA 19137

General Electric Company
Flight Propulsion Lab. Dept.
Attn: D. Suichu
Cincinnati, OH 45215

Bureau of Naval Weapons
Department of the Navy
Attn: Library
Washington, DC

Marquardt Corporation
16555 Saticory Street
Box 2013 - South Annex
Van Nuys, CA 91409

Massachusetts Institute of Tech.
Department of Mechanical Engr.
Attn: T. Y. Toong
77 Massachusetts Avenue
Cambridge, MA 02139

McDonald Douglas Corporation
McDonnell Douglas Astronautics Co.
Attn: William T. Webber
5301 Bolsa Ave.
Huntington Beach, CA 92647

D. E. Mock
Advanced Research Projects Agency
Washington, DC 20525

Lockheed Aircraft Corporation
Lockheed Propulsion Co., Div.
Attn: Norman S. Cohen
P. O. Box 111
Redlands, CA 92373

Naval Postgraduate School
Department of Aeronautics
Attn: David W. Netzer
Monterey, CA 93940

Naval Underwater Systems Center
Energy Conversion Dept.
Attn: Robert S. Lazar, Code 5B331
Newport, RI 02840

Georgia Institute of Technology
School of Aerospace Engineering
Attn: Warren C. Strahle
Atlanta, GA 30332

Georgia Institute of Technology
School of Aerospace Engineering
Attn: Ben T. Zinn
Atlanta, GA 30322

Melvin Gerstein
P. O. Box 452
Altadena, CA 91001

Ohio State University
Department of Aeronautical and
Astronautical Engineering
Attn: R. Edse
Columbus, OH 43210

Pennsylvania State University
Mechanical Engineering Dept.
Attn: G. M. Faeth
207 Mechanical Engineering Bldg.
University Park, PA 16802

Princeton University
Forrestal Campus Library
Attn: Irvin Glassman
P. O. Box 710
Princeton, NJ 08450

Princeton University
Forrestal Campus Library
Attn: David T. Harrje
P. O. Box 710
Princeton, NJ 08540

Princeton University
Forrestal Campus Library
Attn: Martin Summerfield
P. O. Box 710
Princeton, NJ 08540

Propulsion Sciences, Inc.
Attn: Vito Agosta
P. O. Box 814
Melville, NY 11746

Georgia Institute of Technology
School of Aerospace Engineering
Attn: Edward W. Price
Atlanta, GA 30332

Naval Weapons Center
Attn: Charles J. Thelan, Code 4305
China Lake, CA 93555

Naval Postgraduate School
Department of Aeronautics
Attn: Allen F. Fuhs
Monterey, CA 93940

Research and Development Associates
Attn: Raymond B. Edelman
P. O. Box 3580
525 Wilshire Blvd.
Santa Monica, CA 90402

Rockwell International Corp.
Rocketdyne Division
Attn: L. P. Combs, D/991-350
Zone 11
6633 Canoga Avenue
Canoga Park, CA 91304

Rockwell International Corp.
Rocketdyne Division
Attn: James A. Nestlerode
Dept. 596-124, AC46
6633 Canoga Ave.
Canoga Park, CA 91304

Rockwell International Corp.
Rocketdyne Division
Attn: Carl L. Oberg
Dept. 589-197-SS11
6633 Canoga Ave.
Canoga Park, CA 91304

Rockwell International Corp.
Rocketdyne Division
Attn: Library Dept. 596-306
6633 Canoga Avenue
Canoga Park, CA 91304

Purdue University
Jet Propulsion Laboratory
Project Squid
Attn: Robert Goulard
West Lafayette, IN 47907

Purdue University Res. Foundation
School of Mechanical Engineering
Attn: John R. Osborn
Thermal Sci. Propulsion Center
West Lafayette, IN 47906

Tennessee Technological University
Dept. of Mech. Engrg.
Attn: Kenneth R. Purdy
P. O. Box 5014
Cookeville, TN 38501

Textron, Inc.
Bell Aerospace, Div.
Research Department
Attn: John R. Morgenthaler, C-84
P. O. Box One
Buffalo, NY 14240

TRW, Inc.
TRW Systems Gp.
Attn: A. C. Ellings
One Space Park
Redondo Beach, CA 90278

TRW Systems
Attn: G. W. Elveran
One Space Park
Redondo Beach, CA 90278

TRW Systems Group
STL Tech. Lib. Doc. Acquisitions
One Space Park
Redondo Beach, CA 90278

Stanford Research Institute
333 Ravenswood Avenue
Menlo Park, CA 94025

Susquehanna Corporation
Atlantic Research Division
Attn: Library
Shirley Highway and Edsall Rd.
Alexandria, VA 22314

TISIA
Defense Documentation Center
Cameron Station, Bldg. 5
5010 Duke Street
Alexandria, Va. 22314

United Aircraft Corporation
Pratt & Whitney Aircraft Div.
Attn: Thomas C. Mayes
P. O. Box 2691
West Palm Beach, FL 33402

United Aircraft Corporation
United Technology Center
Attn: Library
P. O. Box 358
Sunnyvale, CA 94088

University of California, Berkeley
Dept. of Mechanical Engineering
Attn: A. K. Oppenheim
Berkeley, CA 94720

University of Michigan
Attn: James A. Nicholls
P. O. Box 622
Ann Arbor, MI 48107

University of Wisconsin
Mechanical Engineering Dept.
Attn: P. S. Myers
1513 University Avenue
Madison, WI 53706

Office of Assistnat Director
(Chemical Technician)
Office of the Director of Defense
Research & Engineering
Washington, DC 20301

Tulane University
Attn: J. C. O'Hara
6823 St. Charles Ave.
New Orleans, LA 70118

Ultrasystems, Inc.
Attn: Thomas J. Tyson
500 Newport Center Dr.
Newport Beach, CA

United Aircraft Corp.
Pratt & Whitney Division
Florida Research & Development
Center
Attn: Library
West Palm Beach, FL 33402

United Aircraft Corporation
Attn: R. H. Woodward Waesche
400 Main Street
East Hartford, CT 06108

University of California
Aerospace Engineering Dept.
Attn: F. A. Williams
P. O. Box 109
LaJolla, CA 92037

University of Illinois
Aeronautics/Astronautic Eng. Dept.
Attn: R. A. Strehlow
Trans. Bldg., Room 101
Urbana, IL 61801

University of Utah
Dept. of Chemical Engineering
Attn: Alva D. Baer
Bark Bldg., Room 307
Salt Lake City, UT 84112

U. S. Naval Research Laboratory
Director (Code 6180)
Attn: Library
Washington, DC 20390

Virginia Polytechnic Institute
State University
Attn: J. A. Schetz
Blacksburg, VA 24061